www.sospublication.co.in

Journal of Advanced Laboratory Research in Biology

We- together to save yourself society

e-ISSN 0976-7614

Volume 2, Issue 3, July 2011

Research Article

NADPH Oxidase has a Regulatory Role in Acute Allergic Asthma

Ena Ray Banerjee[1,2*] and William R. Henderson Jr.[1]

[1]*Department of Medicine, Division of Allergy and Infectious Diseases, Center for Allergy and Inflammation, University of Washington, Room 254, 815 Mercer Street, Seattle, WA 98195, USA.*

[1,2*]*Department of Zoology, University of Calcutta, 35 Ballygunge Circular Road, Kolkata-700019, West Bengal, India.*

Abstract

Objective: For the establishment of inflammation, a constant interplay between different effector cells from circulation, local resident cells, soluble mediators and genetic host factors is required. Molecular mechanisms, initiating and perpetuating inflammation, in particular, the involvement of effector cells in redox reactions for producing O_2^- (superoxide anion) through the mediation of NADPH oxidase is a critical step. Prior data suggest that reactive oxygen species (ROS) produced by NADPH oxidase homologues in non-phagocytic cells play an important role in the regulation of signal transduction, while macrophages use a membrane-associated NADPH oxidase to generate an array of oxidizing intermediates which inactivate MMPs on or near them.

Materials, Methods and Treatment: To clarify the role of NADPH oxidase in T cell-initiated, macrophage-associated allergic asthma, we induced allergen dependent inflammation in a gp91^{phox}-/- mouse.

Results: Both inflammation and airway hyperreactivity were more extensive than in wildtype mice post-OVA. Although OVA-specific IgE in plasma were comparable in wildtype and knockout mice, enhanced inflammatory cell recruitment from circulation and cytokine release in lung and BALf, accompanied by higher airway resistance as well as Penh in response to methacholine, indicates a regulatory role for NADPH oxidase in development of allergic asthma. While T cell-mediated functions like Th2 cytokine secretion, and proliferation to OVA were up-regulated synchronous with the overall robustness of the asthma phenotype, macrophage up-regulation in functions such as proliferation, mixed lymphocyte reaction, and MCP-1 directed chemotaxis, but downregulation of respiratory burst response indicates a forking in their signaling pathways. gp91^{phox}-/- MMP12 double knockout (DKO) mice show a similar phenotype as the gp91^{phox}-/- showing the non-involvement or synergistic involvement of MMP12 in the response pathway. In mixed lymphocyte reaction using the Increased B7.1 but reduced B7.2 and MHC class II expression indicating alteration of co-stimulatory molecule expression critical for T cell activation on both gp91^{phox}-/- and DKO mice may explain the mechanism by which gp91^{phox} may regulate Th2 pathway in allergic asthma.

1. Introduction

Asthma is a complex syndrome with well described pathology. However, animal and clinical studies in humans continue to provide conflicting data on the contribution of local cells viz. airway epithelial, endothelial and smooth muscle cells, fibroblasts etc. vs. cells recruited from the circulation. Asthma is characterized by accumulation of inflammatory cells in the lung and airways, secretion of predominantly Th2 cytokines in the lung and airways, epithelial desquamation, goblet cell hyperplasia, mucus hypersecretion and thickening of submucosa resulting in bronchoconstriction and airway hyperresponsiveness. Dysregulated immunity seems to suppress Th1 response and triggers Th2 response whose development is promoted by antigen presenting cells. Th2 cytokines (IL-4, 5, 9, 13) from these cells of which Il-4 and 13 promote B cell differentiation into plasma cells that secrete IgE. Cross-linking of IgE receptors on mast cell releases histamines, prostaglandins, thromboxane and leukotrienes leading to bronchoconstriction, vasodilation and mucus secretion. A cascade of interactions between cells and soluble molecules result in bronchial mucosal inflammation and lead to airway hyperresponsiveness.

*Corresponding author:
E-mail: enarb1@gmail.com; Phone: 91-33-24615445 (Extn. -275); Fax: 91-33-22413222.

The production of superoxide anions (O_2^-) by neutrophils and other phagocytes is an important step in our body's innate immune response. O_2^- is the precursor of a range of chemicals generally referred to as ROS (reactive oxygen species) [1]. These act as microbicidal agents and kill invading microorganisms either directly or through the activation of proteases [2, 3]. O_2^- is produced by the NADPH oxidase, a multi-protein enzyme complex, which is inactive in resting phagocytes, but becomes activated after the interaction of the phagocyte with pathogens and their subsequent engulfment in the phagosome [4]. Defects in the function of the NADPH oxidase result in a severe immunodeficiency, and individuals suffering from CGD (chronic granulomatous disease), a rare genetic disorder that is caused by mutations in NADPH oxidase genes, are highly susceptible to frequent and often life-threatening infections by bacteria and fungi [5]. The microbicidal activity of ROS has generally been seen as the only beneficial function of these chemicals, and uncontrolled production of ROS has been implicated in tissue destruction and a number of disease states. However, over the last couple of years, it has become apparent that ROS produced by NADPH oxidase homologues in non-phagocytic cells also play an important role in the regulation of signal transduction, often via modulation of kinase and phosphatase activities or through gene transcription [6]. These NADPH oxidase homologues are referred to as Nox enzymes ($gp91^{phox}$ is specified as Nox2; where phox is phagocytic oxidase), and several members of this novel protein family have been identified so far.

There is increasing evidence that redox regulation of transcription, particularly activator protein-1 (AP-1) and nuclear factor kappa B (NF-κB), is important in inflammatory diseases. NADPH oxidase, the primary source of reactive oxygen species is a strong candidate for the development of therapeutic agents to ameliorate inflammation and end-organ damage. The possibility of gene therapy for inherited diseases with a single gene mutation had been verified by the successful treatment with bone marrow transplantation. As the gene therapy method and theory have progressed rapidly, it is expected that gene therapy will overcome the complications of bone marrow transplantation. Of these inherited diseases, chronic granulomatous disease (CGD) is one of the most expected diseases for gene therapy. CGD is an inherited immune deficiency caused by mutations in any of the following four phox genes encoding subunits of the superoxide-generating phagocyte NADPH oxidase. It consists of membranous cytochrome b558 composed of $gp91^{phox}$ and $p22^{phox}$, and four cytosolic components, $p47^{phox}$, $p67^{phox}$, rac p21 and $p40^{phox}$, which translocate to the membrane upon activation. The $gp91^{phox}$ subunit (also called the □-subunit of the cytochrome) consists of 570 amino acids and has a molecular mass of 65.3 kDa, but runs as a broad smear of approx. 91 kDa on SDS/polyacrylamide gels due to a heterogeneous glycosylation pattern of three asparagine residues (Asn^{132}, Asn^{149}& Asn^{240}) [7].

The N-terminal 300 amino acids are predicted to form six transmembrane α-helices, while the C-terminal cytoplasmic domain contains the binding sites for FAD and NADPH, shown experimentally through cross-linking studies and the observation that relipidated flavocytochrome alone can generate O_2^- []. In addition, $gp91^{phox}$ is responsible for complexing the two non-identical haem groups of the NADPH oxidase via two histidine pairs. Hence $gp91^{phox}$ contains all cofactors required for the electron transfer reaction which occurs in two steps. First, electrons are transferred from NADPH on to FAD and then to the haem group in the second step to reduce O_2 to O_2^- in a one-electron-transfer reaction. At present, no information is available on the three-dimensional structure of $gp91^{phox}$ or fragments thereof, although a model for the structure of the cytoplasmic domain of $gp91^{phox}$ has been suggested based on sequence homology with the FNR (ferredoxin–NADP reductase) family [High-resolution structure of the nitrile reductase QueF combined with molecular simulations provide insight into enzyme mechanism [8]. Significant insight into the topology of the cytochrome and the sites of interaction with other oxidase components has been gained through the use of a number of techniques, including epitope mapping or random sequence peptide phage analysis []. Additionally, the study of cytochrome isolated from patients with X-linked CGD has contributed to our current understanding of its function [9].

Involvement of the $gp91^{phox}$ subunit in oxidative burst response by PMNs as well as Mϕs is not clear. Macrophages use a membrane-associated NADPH oxidase to generate an array of oxidizing intermediates. In some studies, it has been demonstrated that oxidants potently and efficiently inactivate matrilysin (MMP-7) by cross-linking adjacent tryptophan-glycine residues within the catalytic domain of the enzyme. These *in vitro* observations suggest that MMP inactivation can occur on or near phagocytes that produce both MMPs and reactive intermediates. In the absence of reactive intermediates, the unrestrained proteolytic activity might lead to detrimental tissue damage. Indeed, inherited deficiency of $gp91^{phox}$, a phagocyte-specific component of the NADPH oxidase required for oxidant production, and targeted deletion of its mouse homologue result in granuloma formation and excessive tissue destruction [10]. Aberrant regulation of MMP activity may contribute to the damage that occurs when phagocytes are unable to generate oxidants. $gp91^{phox}$ mutant mice were found to develop spontaneously, progressive emphysema, equal to that seen in smoke-exposed wild-type animals. Macrophages and neutrophils use membrane-associated NADPH oxidase to generate reactive oxygen intermediates. The initial product of the NADPH oxidase is superoxide, which is converted into oxidizing oxygen and nitrogen species.

Because their characteristic end products have been detected in diseases ranging from atherosclerosis to neurodegenerative disorders, reactive oxygen and nitrogen intermediates are thought to contribute to inflammatory tissue injury. However, humans and animals deficient in phagocyte NADPH oxidase tend to form granulomas and to have excessive tissue destruction and an exuberant inflammatory response, raising the possibility that oxidants derived from white cells actually govern or suppress inflammation.

One potential mechanism whereby reactive oxygen species can influence inflammation and the associated tissue damage is by regulating the activity of MMPs. In addition to their ability to act on extracellular matrix, MMPs can affect inflammation by directly or indirectly regulating the activity of inflammatory mediators such as chemokines. Because reactive intermediates effectively inactivate MMPs *in vitro*, they provide an efficient mechanism for inhibiting unregulated catalysis by these extracellular proteinases, thereby preventing pathological destruction of tissue proteins and exuberant inflammation. Production of reactive intermediates by the phagocyte NADPH oxidase could confine MMP activity in space and time, permitting only bursts of pericellular proteolysis.

This study addresses for the first time the relationship between $gp91^{phox}$ and MMP in the development of T cell-mediated acute allergic asthma in a mouse model using genetic knockout mice, $gp91^{phox}$-/- which will be referred to as NOX-/- and MMP12NOX double knockout. The study shows that gp91phox most likely has a regulatory role in the onset and maintenance of the composite asthma phenotype in mouse and deletion of $gp91^{phox}$ may alter expression of co-stimulatory/co-inhibitory molecules B7.1 (increased) and B7.2 (decreased) and MHCII expression (increased) which may explain the mechanism by which macrophages despite increased migration to the inflammatory foci *in vivo* and increased migration in a chemotaxis chamber to MCP-1, and enhanced proliferation to syngeneic or allogeneic stimulus, fail to show oxidative burst response. MMP12 seems to be either the innocent bystander, not contributing to the overall asthma phenotype or has a synergistic (not additive) role in the process.

2. Materials and Methods

2.1 Mice

Both $gp91^{phox-/-}$ mice [11] (Jackson Laboratories, Bar Harbor, ME) and $mmp12^{-/-}$ mice were on a C57Bl/6J background and had been outcrossed and then intercrossed for three generations to generate animals deficient in both genes [12]. C57BL6 mice (Taconic) were used as the control group and are called wild type. In total the following numbers of animals were used in each group:

n	WT	NOX-/-	MMP12NOX-/-
Control (+Alum)	14	14	16
+OVA	16	15	14

2.2 Allergen sensitization and challenge

Mice were sensitized and later challenged with OVA (Pierce, Rockford, IL) as described previously (2). Mice were immunized with OVA (100μg) complexed with aluminium sulfate in a 0.2-ml volume, administered by i.p. Injection on day 0. On days 8 (250μg of OVA) and on days 15, 18, and 21 (125μg of OVA), mice were anesthetized briefly with inhalation of isoflurane in a standard anesthesia chamber and given OVA by intratracheal (i.t.) administration. Intratracheal challenges were done as described previously (Iwata A, JI, 2001). Mice were anesthetized and placed in a supine position on the board. The animal's tongue was extended with lined forceps and 50μl of OVA (in the required concentration) was placed at the back of its tongue. The control group received normal saline with aluminium sulfate by i.p. route on day 0 and 0.05ml of 0.9% saline by i.t. route on days 8, 15, 18, and 21.

2.3 Pulmonary function tests

In vivo airway, hyperresponsiveness to methacholine was measured 24 hours after the last OVA challenge by both invasive and non-invasive plethysmography.

2.4 Invasive plethysmography

On d 22, 24 h after the last intratracheal allergen (OVA) challenge invasive pulmonary mechanics were measured in mice in response to methacholine in the same manner as previously described [13-17] with the following modifications:

a) The thorax was not opened,
b) Mice were ventilated with a tidal volume of 200μl and respiratory rate of 120 breaths/min using a MiniVent Ventilator for Mice (Harvard Apparatus, Holliston, MA),
c) Mice received aerosolized solutions of methacholine (0, 3.125, 6.25, 12.5, 25, 50, and 100mg/ml in normal saline) via an AER 1021 nebulizer aerosol system (Buxco Electronics, Inc., Wilmington, NC) with 2.5-4 micron aerosol particle size generated by NEB0126 nebulizer head (Nektar Therapeutics, San Carlos, CA), and
d) A commercial plethysmography system (Model PLY4111 plethysmograph, MAX II amplifier and pressure transducer system, and Biosystem XA software, Buxco Electronics, Inc.) was used to determine R_L as calculated from measures of pressure and flow and expressed as $cmH_2O/ml/s$). Non-invasive plethysmography (expressed as Penh) was also assessed on d 22 in independent experiments.

2.5 Noninvasive whole body plethysmography

In conscious, freely moving, spontaneously breathing mice using whole-body plethysmography (model PLY 3211; Buxco Electronics, Sharon, CT) as previously described (Henderson, W.R., 2005, J.

Allergy Clin. Immunol.). Mice were challenged with aerosolized saline or increasing doses of methacholine (5, 20, and 40mg/ml) generated by an ultrasonic nebulizer (DeVilbiss Health Care, Somerset, PA) for 2 min. The degree of bronchoconstriction was expressed as enhanced pause (P_{enh}), a calculated dimensionless value, which correlates with the measurement of airway resistance, impedance, and intrapleural pressure in the same mouse. P_{enh} readings were taken and averaged for 4 min after each nebulization challenge. P_{enh} was calculated as follows: P_{enh}=[(Te/Tr-1)X (PEF/PIF), where T_e is expiration time, T_r is relaxation time, PEF is peak expiratory flow, and PIF is peak inspiratory flow X 0.67 coefficient. The time for the box pressure to change from a maximum to a user-defined percentage of the maximum represents the relaxation time. The T_r measurement begins at the maximum box pressure and ends at 40%.

2.6 BAL

After pulmonary function testing, the mouse underwent exsanguination by intraorbital arterial bleeding and then BAL (0.4ml three times) of both lungs. Total BAL fluid cells were counted from a 50μl aliquot and the remaining fluid was centrifuged at 200*g* for 10 min at 4^0C and the supernatants stored at -70^0C for assay of BAL cytokines later. The cell pellets were resuspended in FCS and smears were made on glass slides. The cells, after air drying, were stained with Wright-Giemsa (Biochemical Sciences Inc, Swedesboro, NJ) and their differential count was taken under a light microscope at 40X magnification. Cell number refers to that obtained from lavage of both lungs/mouse.

2.7 Lung parenchyma

Lung mincing and digestion was performed after lavage as described previously (Labarge S. *et al.*,) with 100u/ml collagenase for 1 hour at 37^0C, and filtered through a 60# sieve (Sigma). All numbers mentioned in this paper refer to cells obtained from one lung/mouse.

2.8 Lung histology

Lungs of other animals of the same group were fixed in 4% paraformaldehyde overnight at 4^0C. The tissues were embedded in paraffin and cut into 5μm sections. A minimum of 15 fields was examined by light microscopy. The intensity of cellular infiltration around pulmonary blood vessels was assessed by Hematoxylin and Eosin staining. Airway mucus was identified by staining with Alcian blue and Periodic Acid Schiff staining as described previously [13-17].

2.9 Fluorescein-activated cell sorter (FACS) analysis

Cells from hemolysed peripheral blood (PB), bone marrow (BM), bronchoalveolar lavage (BAL), lung parenchyma (LP), spleen, mesenteric lymph nodes (MLN), cervical lymph nodes (CLN), axillary lymph nodes (LNX) and inguinal lymph nodes (LNI) were analyzed on a FACSCalibur (BD Immunocytometry Systems, San Jose, CA) by using the CELLQuest program. Staining was performed by using antibodies conjugated to fluorescein isothiocyanate (FITC), phycoerythrin (PE), allophycocyanin (APC), Peridinin Chlorophyll Protein (Per CP-Cy5.5) and Cy-chrome (PE-Cy5 and PE-Cy7). The following BD Pharmingen (San Diego, CA) antibodies were used for cell surface staining: APC-conjugated CD45 (30F-11), FITC-conjugated CD3 (145-2C11), PE-Cy5 conjugated CD4 (RM4-5), PE-conjugated CD45RC (DNL-1.9), APC-conjugated CD8 (53-6.7), PE-Cy5 conjugated B220 (RA3-6B2), FITC-conjugated IgM, PE-conjugated CD19 (ID3), PE-conjugated CD21 (7G6), FITC-conjugated CD23 (B3B4), APC-conjugated GR-1 (RB6-8C5), and PE-conjugated Mac1 (M1/70). PE-Cy5 conjugated F4/80 (Cl:A3-1(F4/80)) was obtained from Serotec Ltd., Oxford, UK. PE-conjugated anti-α4 integrin (PS2) and anti-VCAM-1(M/K-2) was from Southern Biotechnology, Birmingham, Ala. Irrelevant isotype-matched antibodies were used as controls.

2.10 CFU-c assay

To quantitate committed progenitors of all lineages, CFU-c assays were performed using methylcellulose semisolid media (Stemgenix, Amherst, N.Y.) supplemented with an additional 50ng of stem cell factor (Peprotech, Rocky Hill, N.J.) per ml. Next, 50,000 cells from bone marrow, 500,000 cells from spleen, 0.01 million cells from lung and BAL, and 10μl peripheral blood were plated on duplicate 35-mm culture dishes and then incubated at 37°C in a 5% CO_2-95% air mixture in a humidified chamber for 7 days. Colonies generated by that time were counted by using a dissecting microscope, and all colony types (i.e., burst forming units-erythroid [BFU-e], CFU-granulocyte-macrophage [CFU-GM], and CFU-mixed [CFU-GEMM]) were pooled and reported as total CFU-C. Total CFU-c per organ was calculated by extrapolating CFU-c against a number of plated cells to the total number of cells in the organ.

2.11 ELISA for cytokines

Th2 cytokines (IL-4 and 5) and TNFα and IFNγ in BAL and serum (previously frozen at -80^0C) were outsourced to Lincoplex Biomarker Immunoassays, Millipore. IL-13 was measured by Quantikine M kits from R&D Systems, Minneapolis, MN.

2.12 OVA-specific IgE and IgG1 in serum

Anti-mouse IgE (R35-72) and IgG1 (A85-1) from BD Biosciences, San Diego, CA were used for measuring OVA-specific IgE and IgG1 (in serum previously frozen at -70^0C) respectively by standard ELISA procedures as previously described [17].

2.13 Chemotaxis assay

Chemotaxis assay was performed with 10 million macrophages pooled from 4 mice/experimental group.

Macrophages were prepared by adhering BALf cells in high glucose medium for 2 hours followed by detachment by mechanical scraping and resuspension in Phenol red-free high glucose DMEM (Gibco) with 5% FBS with 0.5μg/ml Calcein-AM (1:2000 dilution) and incubation for 20 min at 37^0C. MCP-1 at dilutions ranging from 0.1-25mM was used and 15mM was taken to be the optimum dose. 96 well Neuroprobe CTX plates (Chemicon, Temecula< CA) were used. 29μl MCP-1 (15mM) was added as a single convex drop and the polycarbonate filter placed gently over it and incubated at 37^0C for 30 min. The cell suspension was added in designated slots over the filter membrane also in 29μl volume. The chamber was incubated at 37^0C in a humidified CO_2 incubator for 2h. Excess cells were wiped off with kimwipes at the end of the incubation period. Migrated cells were quantified by fluorescence (excitation at 488nm, emission at 520nm) using a Victor 3V (Perkin Elmer laboratories) using a Wallac1420 software.

2.14 Mouse model of pulmonary fibrosis

A single intratracheal dose of 0.075U/ml of bleomycin in 40μl saline was administered (d 0), and mice were sacrificed 14 and 21d later. Mice C57Bl/6 were kept under ABSL-2 conditions approved by the IACUC of the University of Washington and monitored daily. They were housed under specific pathogen-free condition and were given food and water *ad libitum.* They were sacrificed on d 14. 1 week after bleomycin administration, mice developed marked interstitial and alveolar fibrosis, detected in lung sections by Masson's trichrome stain. Analysis of cell populations by enzymatic digestion by collagenase Type IV followed by cell counting in Coulter counter and subsets identified and quantified by FCM and total and differential count of H&E stained cytospin smears of single cell suspensions show loss of type II and type I alveolar epithelial cells and influx of macrophages. AEI and II were isolated following standard protocol.

2.15 Real time-PCR analysis

For real-time PCR analysis of mRNA expression of particular genes in differentiating human ESC as well as in the lungs of recipient animals in transplantation experiments, total RNA was extracted from cells (<500/sample) by PicoPure RNA isolation kit from Arcturus, Mountainview, CA and those from lungs (kept in RNAlater (Ambion) at -80^0C), by RNA extraction kit (RNeasy) from Qiagen and cDNA made from it using a Superscript III system from Invitrogen. The PCR reaction solution contained 0.5μg of total RNA, 6-mM magnesium chloride, and 0.5-μM of each primer (primer oligo sequences are in Table 1). Other components in the reverse transcriptase–PCR master mix included buffer, enzyme, SYBR Green I, and deoxyribonucleotide triphosphate. For reverse transcription, the 20μL of reaction capillaries were incubated at 50^0C for 2 min followed by a denaturation at 95^0C for 10 min. Polymerase chain reaction by an initial denaturation at 95^0C for 15 s and then annealing at 60^0C 1 min, repeat 45 cycles. Finally, a melting curve analysis was performed by following the final cycle with incubation at 95^0C for 15 s, at 60^0C for 15 s, then 95^0C for 15 s. Negative control samples for the reverse transcriptase–PCR analysis, which contained all reaction components except RNA, were performed simultaneously to determine when the nonspecific exponential amplification cycle number was reached. Forward and reverse primers are as in Table 1and were synthesized by the University of Washington Biochemistry services using the Primer Express software. PCR was carried out using the comparative Ct method (Applied Biosystems software) with SYBR Green PCR core reagents (Applied Biosystems) and analysed using Applied Biosystems 7900HT Real-Time PCR System software SDS 2.2.1.

Table 1. List of mouse primers for real-time PCR.

Cell marker	Gene	Forward primer	Reverse primer
House-keeping genes	GAPDH	CGTCCCGTAGACAAAATGGT	TCAATGAAGGGGTCGTTGAT
	β-actin	GTGGGCCGCTCTAGGCACCAA	CTCTTTGATGTCACGCACGATTTC
Cytokine genes	IFN-γ	GCGTCATTGAATCACACCTG	TGAGCTCATTGAATGCTTGG
	IL-1α	TCAAGATGGCCAAAGTTCCT	TGCAAGTCTCATGAAGTGAGC
	IL-1β	TGAAGCAGCTATGGCAACTG	GGGTCCGTCAACTTCAAAGA
	IL-2	AACCTGAAACTCCCCAGGAT	CGCAGAGGTCCAAGTTCATC
	IL-3	CCGTTTAACCAGAACGTTGAA	CCACGAATTTGGACAGGTTT
	IL-4	GGCATTTTGAACGAGGTCAC	AAATATGCGAAGCACCTTGG
	IL-5	ATGGAGATTCCCATGAGCAC	AGCCCCTGAAAGATTTCTCC
	IL-6	AACGATGATGCACTTGCAGA	GGTACTCCAGAAGACCAGAGGA
	IL-10	TGAATTCCCTGGGTGAGAAG	TGGCCTTGTAGACACCTTGG
	IL-12β	ATCGTTTTGCTGGTGTCTCC	CATCTTCTTCAGGCGTGTCA
	IL-13	CCTCTGACCCTTAAGGAGCTT	ATGTTGGTCAGGGAATCCAG
	MCP-3	TCTGTGCCTGCTGCTCATAG	CTTTGGAGTTGGGGTTTTCA
Growth factor genes	TGFβ2	GGAGGTTTATAAAATCGACATGC	GGCATATGTAGAGGTGCCATC
	VEGFa	TACCTCCACCATGCCAAG	TGGTAGACATCCATGAACTTGA
	VEGFb	GGCTTAGAGCTCAACCCAGA	TGGAAAGCAGCTTGTCACTTT
	VEGFc	GGGAAGAAGTTCCACCATCA	TCGCACACGGTCTTCTGTAA

Table 2A. Leukocyte subsets (x10^6) in blood, lungs and BAL fluid post OVA treatment.

	Blood							
	Total WBCs	Lymphocytes		Monocytes	Neutrophils	Eosinophils	Basophils	
		CD3+	B220+					
WA	11.9±2.4	5.54±1.17	3.08±1.05	0.38±0.185	3.648±0.184	0.223±0.014	0.066±0.001	
WO	24.72±6.41	7.31±1.31	5.93±1.17	1.62±0.35	7.97±1.14	0.74±0.36	1.05±0.02	
NOXA	14.2±3.012	5.7±1.865	2.99±1.033	0.77±0.053	4.56±1.074	0.133±0.043	0.028±0.002	
NOXO	25.625±4.063	6.186±1.076	6.742±0.964	2.424±1.076	8.741±0.064	1.061*±0.004	0.556±0.003	
DKOA	11.7±2.76	4.69±1.06	2.467±0.96	0.63±0.12	3.74±1.27	0.106±0.07	0.02±0.001	
DKOO	27.56±2.79	6.61±1.49	7.27±2.01	2.6±0.47	9.39±2.44	1.14*±0.46	0.59±0.14	
	Lungs							
	Total WBCs	Lymphocytes		Monocytes	Neutrophils	Eosinophils	Basophils/ Mast cells	Mϕ
		CD3+	B220+					
WA	1.86±0.543	0.179±0.021	0.035±0.002	0.826±0.054	0.319±0.054	0	0	0.497±0.015
WO	12.35±3.96	4.87±1.05	0.09±0.01	0.37±0.09	1.47±0.43	2.22±0.76	0.046±0.012	3.09±1.08
NOXA	5.49$^{\#}$±1.064	0.446$^{\#}$±0.002	0.113$^{\#}$±0.001	2.593$^{\#}$±0.76	0.892$^{\#}$±0.011	0	0	1.489$^{\#}$±0.016
NOXO	22.6*±7.544	4.084±1.075	1.29*±0.643	3.171*±1.075	4.337*±1.074	4.102*±1.066	0.089*±0.002	5.682±0.064
DKOA	3.78$^{\#}$±1.07	0.3±0.14	0.07±0.01	1.78$^{\#}$±0.54	0.61±0.02	0.001±0.0001	0	1.02$^{\#}$±0.29
DKOO	21.66*±408	3.89±1.06	0.43*±0.16	3.03*±0.89	4.16*±1.33	3.93*±1.13	0.08 *±0.002	5.44*±1.26
	BAL fluid (2 lungs)							
WA	0.8±0.013	0	0	0.013±0.004	0	0	0	0.787±0.011
WO	9.46±0.89	1.64±0.21	1.54±0.021	1.26±0.03	0.86±0.01	4.26±0.07	0.04±0.002	0.56±0.004
NOXA	0.63±0.018	0	0	0.014±0.002	0	0	0	0.616±0.003
NOXO	16*±3.159	2.04±0.754	1.213±0.003	2.08±0.074	2.427*±1.066	6.741*±2.076	0.051±0.001	1.568*±0.72
DKOA	0.865±0.01	0	0	0.025±0.002	0	0	0	0.84±0.18
DKOO	15.89*±4.03	2±0.86	1.22±0.66	2.05±0.75	2.415*±1.01	6.67*±1.14	0.05±0.003	1.55*±0.63

Number of cells (x10^6) of leukocyte subsets in peripheral blood, lung parenchyma and bronchoalveolar lavage fluid (BALf).Total white blood cells were counted by a Beckman Coulter particle counter and subsets quantified using specific antibody staining in FACS and corroborated by morphological assessment by light microscopy and also by hemavet using the specifics of mouse. The table shows data averaged from three independent experiments ± SEM. * denotes p value<0.05 compared to values from post-OVA wildtype mice and # denotes p value<0.05 compared to alum-treated wildtype. Abbreviations used are: WA=wildtype +alum, WO= wildtype + OVA, NOXA=gp91^{phox}-/- + alum, NOXO=gp91^{phox}-/- + OVA, DKOA= MMP12-gp91^{phox} double knockout + alum, DKOO= MMP12-gp91^{phox} double knockout + OVA. (n=5/group).

Table 2B. Recruitment index: Inflammatory hematopoietic cells found in lungs and BALf expressed as a fraction of corresponding cells in circulation.

		T cells	B cells	Monocytes	Neutrophils	Eosinophils	Basophils
Lungs	WO	0.6	0.015	0.22	0.18	3	0.04
	NOXO	0.6	0.19	1.3	0.49	3.8	0.16
	DKOO	0.58	0.05	1.1	0.44	3.4	0.13
BALf	WO	0.22	0.25	0.77	0.107	5.75	0.03
	NOXO	0.32	0.17	0.85	0.27	6.3	0.09
	DKOO	0.51	0.16	0.78	0.26	5.8	0.08

Number of cells (x10^6) in lungs and BALf were the numerator and the number of cells (x10^6) in circulating blood was the denominator in the fraction calculated to show recruitment index or inflammatory cells recruited from circulation to lung parenchyma and airways in response to the OVA-allergic challenge.

2.16 Statistical analysis

Statistical differences among samples were tested by Student t test. A P value less than 0.05 was considered statistically significant.

3. Results

3.1 The effect of gp91^{phox} deletion on the development of composite asthma phenotype

Composite asthma phenotype developed completely and more aggressively in both gp91^{phox}-/- and MMP12-gp91^{phox} double knockout mice post OVA treatment as described in Fig. 1. Inflammation in terms of total inflammatory migration (measured by FACS of surface marker expression and differential count of H&E stained cytospin smears) was increased (Table 2A). In bone marrow, NOX-/- post OVA has 1.4-fold more cells, in peripheral blood, 1.3-fold more cells, spleen had 1.3-fold more cells, lung parenchyma had 1.8-fold more cells, and BALf: 2-fold more cells compared to post-OVA WT. Of note, 2.4-fold more PMNs, 1.96-fold more B lymphocytes, 5-fold more eosinophils in post-OVA NOX-/- compared to post-OVA WT BALf was found. Overall systemic response, inflammatory recruitment from blood to inflammation in the lung is more (Table 2B).

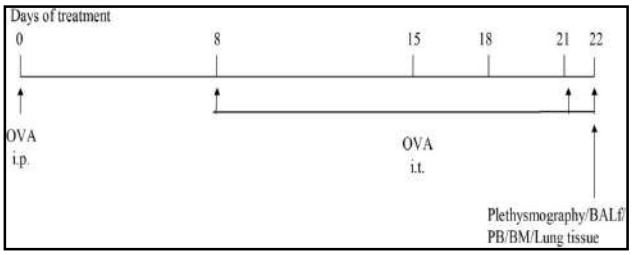

Fig. 1. Study design to generate an acute allergic asthma phenotype in mice: Mice were sensitized with OVA (100μg) complexed with aluminium sulfate in a 0.2-ml volume, administered by i.p. injection

on day 0 and later challenged with OVA On days 8 (250μg of OVA) and on days 15, 18, and 21 (125μg of OVA), (Pierce, Rockford, IL) by intratracheal instillation. Mice were immunized with OVA (100μg) complexed with aluminium sulfate in a 0.2-ml volume, administered by i.p. injection on day 0. The control group received normal saline with aluminium sulfate by i.p. route on day 0 and 0.05ml of 0.9% saline by i.t. route on days 8, 15, 18, and 21. They were sacrificed on d22. The abbreviations used are i.p. intraperitoneal; i.t. intratracheal; BAL, bronchoalveolar lavage; PB, peripheral blood.

3.2 Pulmonary function test

Pulmonary function tests measured by both non-invasive plethysmography and invasive plethysmography (Fig. 2A-C) show 2.5-fold increase in Penh values compared to WT post-OVA at 100mg/ml dose of methacholine. 1.89 and 1.35-folds increase was found in gp91^{phox}-/- and DKO respectively at 100mg/ml dose of methacholine compared to WT post-OVA by invasive plethysmography of anesthetized mice.

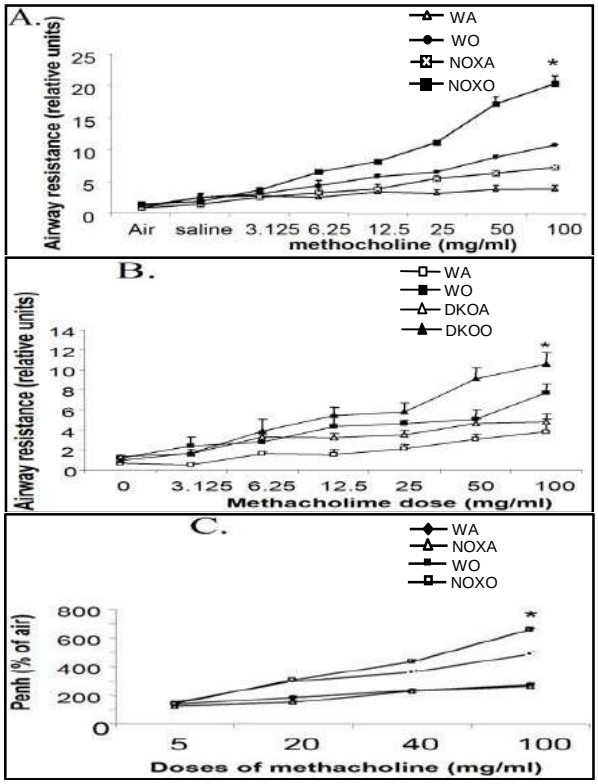

Fig. 2. Pulmonary function testing. A. Airway resistance in WT vs. gp91phox-/-.

B. Airway resistance obtained by invasive plethysmography show increased values in both gp91phox-/- and gp91phoxMM12 double knockout mice compared to wildtype post-OVA.

On d 22, 24 h after the last intratracheal allergen (OVA) challenge invasive pulmonary mechanics were measured using a commercial plethysmography system (Model PLY4111 plethysmograph, MAX II amplifier and pressure transducer system, and Biosystem XA software, Buxco Electronics, Inc.) mice receiving aerosolized solutions of methacholine (0, 3.125, 6.25, 12.5, 25, 50, and 100mg/ml in normal saline) via an AER 1021 nebulizer aerosol system (Buxco Electronics, Inc., Wilmington, NC) with 2.5-4 micron aerosol particle size generated by NEB0126 nebulizer head (Nektar Therapeutics, San Carlos, CA), and RL as calculated from measures of pressure and flow and expressed as cmH_2O/ml/s was determined. Figures show Airway resistance (RL) values ± SEM of data obtained from 3 independent experiments (n=5/group).

C. Non-invasive plethysmography (expressed as Penh) was also assessed on d 22 in independent experiments with gp91phox-/- only and this co-related with the airway resistance values obtained by invasive plethysmography.

For non-invasive plethysmography, mice were challenged with increasing doses of aerosolized methacholine (0, 5, and 20, 40, and 100mg/ml in normal saline) generated by an ultrasonic nebulizer (DeVilbiss Health Care, Inc., Somerset, PA) for 2 min. and the degree of bronchoconstriction was expressed as enhanced pause (Penh), a calculated dimensionless value that correlates with measurement of airway resistance, impedance, and intrapleural pressure. Penh is primarily independent of FRC, tidal volume, and respiratory rate since the ratio of measurements is obtained during the same breath and has a strong correlation with both airway resistance (Raw) measured directly in anesthetized, tracheotomized, and mechanically ventilated mice. *denotes p value<0.01 compared to post-OVA wildtype values.

3.3 Cellularity in bone marrow, blood, lungs and airways

Cellularity was increased in post-OVA mice compared to saline-treated mice**.** Fig. 3 shows 1.8-fold and 1.7-fold increase in the number of cells in lung parenchyma and BALF and 1.4-fold in spleen in both KO mice than WT. Recruitment index (Table 2) was increased in B cells, monocytes, PMNs, eosinophils and basophils in both KO mice post-OVA compared to post-OVA WT.

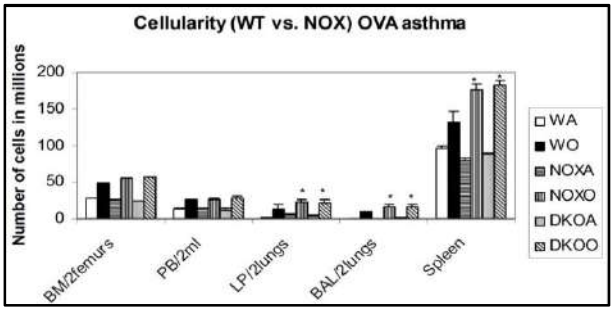

Fig. 3. Increase in total cell number in the lung and BALf of knockout mice compared to post-OVA WT. Cell number was counted using a Z1 particle counter from Beckman Coulter. Bone marrow cells (BM) were flushed out of two femurs, blood (PB) was obtained by infra-orbital bleeding and extrapolated to a 2ml volume as the total volume of blood in a 20gm mouse, from the volume of blood actually obtained, perfused lung was minced and digested with collagenase IV and single cell suspension made of both lungs, and bronchoalveolar lavage fluid (BALf) was obtained from both lungs, and the cell numbers counted. The data shown have been derived from 3 independent experiments and expressed as mean values ± SEM. *denotes p value<0.01 compared to post-OVA wildtype values. Abbreviations used are: WT=wildtype, NOX=gp91^{phox}-/-, DKO=gp91^{phox}-MMP12 double knockout, WA=WT+alum, WO=WT+OVA, NOXA=gp91^{phox}-/-+alum, NOXO=gp91^{phox}-/-+OVA, DKOA= gp91^{phox}-MMP12 double knockout+alum, DKOO= gp91^{phox}-MMP12 double knockout+OVA.

3.4 Progenitors in bone marrow, blood, lungs and airways

Table 3 and Fig. 4 shows decrease in number of colonies forming units in post-OVA bone marrow and

lung of both KO mice compared to similarly treated WT. Progenitor number was however somewhat upregulated in both KO groups post-OVA compared to Post-OVA WT.

Table 3. Decrease in clonogenic potential in bone marrow and lung of both KO mice post-OVA. In gp91^{phox}-/- progenitors in BM decrease by 28.8% while in double knockout, it decreases by 27.9% compared to the values in WT post-OVA. In the lung, the decrease in progenitor number was 1.8-fold and 1.5-fold respectively. Results shown are pooled from three independent experiments (n=5/group) ± SEM. Abbreviations used are BM, bone marrow; PB, peripheral blood, LP, lung parenchyma, BALf, bronchoalveolar lavage fluid. The total number of progenitors was extrapolated to the total number cells obtained from each tissue.

Mean

	PB/2ml	BM/2femurs	LP/2lungs	BAL/2lungs	Spleen
WA	5371.615	17034.5	241.93	3.15	75858.9
WO	16915.61	57161.5	11225.49	5573.875	188275.6
NOXA	2343	8293.32	604.12	59.926	41774.25
NOXO	9403.35	40677.7	6299.337	5921.744	219677.5
DKOA	4591.678	11783.19	562.91	32.932	65974.3
DKOO	9262.11	41278.3	7103.16	6012.22	197822.7

SEM

WA	188.6942	158.8784	115.8199	16.32993	523.0583
WO	219.1485	161.9139	155.0757	41.63332	361.9139
NOXA	244.3471	197.1253	125.8199	19.14854	75.49834
NOXO	382.2598	220.4159	195.9166	41.63332	426.8858
DKOA	256.6731	284.5762	183.7863	45.68423	344.3138
DKOO	342.6876	361.6896	201.5763	59.6876	388.6876

3.5 Inflammation in the lungs

Histopathology showed a marked increase in peribronchiolar and perivascular infiltration of inflammatory cells post-OVA in both KO mice compared to control (Fig. 5 A-C). The photomicrographs show a marked increase in both number of inflammatory cells and mucus secretion in the airways.

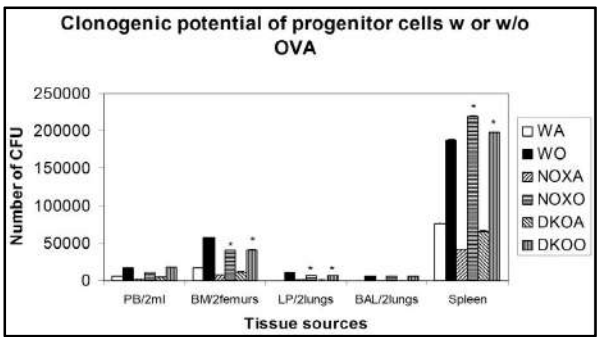

Fig. 4. Clonogenic potential was decreased in the bone marrow and lung progenitors of both knockout mice post OVA. 10ml heparinized whole peripheral blood (PB) obtained by infra-orbital bleeding of anesthetized mouse, 50,000 bone marrow cells (BMC) flushed out of the femurs, 1 million lung parenchyma (LP) cells digested by collagenase IV, 1 million cells from bronchoalveolar lavage fluid (BALf) and 500,000 cells from spleen was plated in 2ml semisolid methylcellulose medium and cultured for 7 d for PB, BM and spleen and for 14d for LP and BALf. Colony forming units (CFU) was counted manually on a Leica DMIL and an Olympus sZX12 inverted microscope. Results shown are pooled from three independent experiments (n=5/group) ± SEM. * denotes p value<0.01 compared to post-OVA wildtype values. Abbreviations used are: WT=wildtype, NOX=gp91phox-/-, DKO=gp91phox-MMP12 double knockout, WA=WT+alum, WO=WT+OVA, NOXA=gp91phox-/-+alum, NOXO=gp91phox-/-+OVA, DKOA= gp91phox-MMP12 double knockout+alum, DKOO= gp91phox-MMP12 double knockout+OVA.

3.6 Airway goblet cell metaplasia

1.27-fold and 1.22-fold increase in percent metaplastic goblet cells (Fig. 6) was measured by counting under light microscope, the blue mucus laden cells around airways vs. the pink squamous cells which do not show metaplasia.

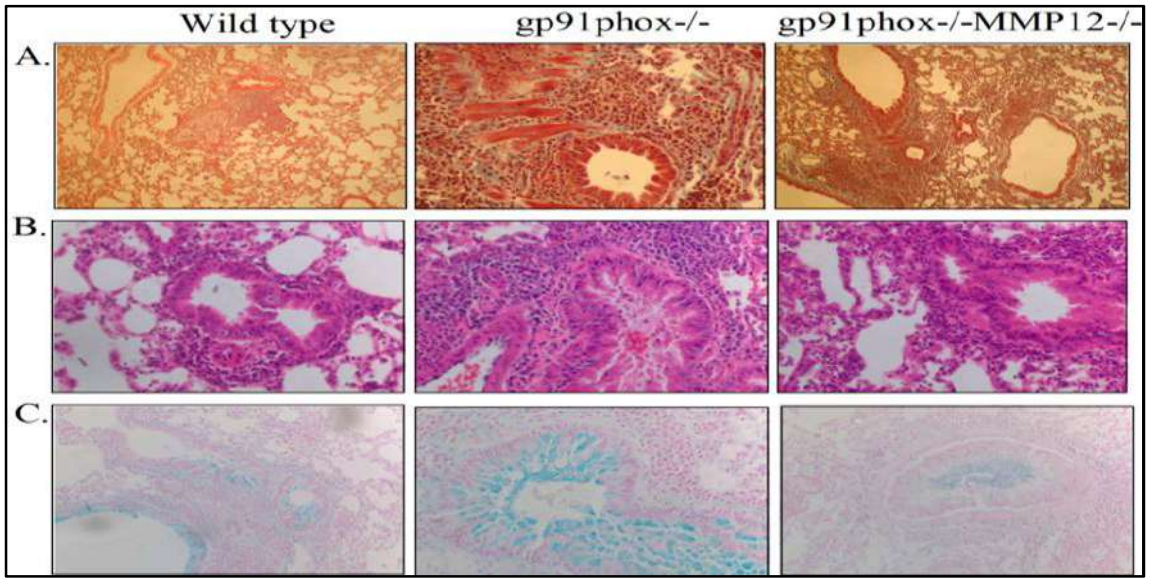

Fig. 5. Both knockout mice show increased inflammation and mucus secretion post OVA compared to WT. Paraffin sections of lungs of OVA-treated mice were stained with A, Hematoxylin and eosin (10X), B. with Masson's Trichrome stain (20X), and C. Alcian blue counterstained with eosin (10X). Sections were viewed with a BX4I Olympus microscope and photomicrographs taken with a Nikon Spot digital camera. Inflammatory cell migration was more pronounced around the airways in the OVA-treated knockout mice compared to control.

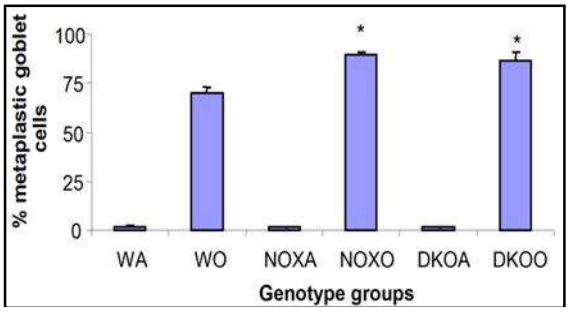

Fig. 6. Increase in percent alcian blue positive cells (goblet cell metaplasia) in gp91^{phox}-/- and gp91^{phox}-MMp12 double knockout (DKO) post-OVA compared to wildtype (WT) post-OVA. Metaplastic goblet cells were counted as the blue cells stained positive by alcian blue. Percent metaplastic goblet cells are calculated from the total number of cells counted around each airway. Abbreviations used are: WT=wildtype, NOX=gp91^{phox}-/-, DKO=gp91^{phox}-MMP12 double knockout, WA=WT+alum, WO=WT+OVA, NOXA=gp91^{phox}-/-+alum, NOXO=gp91^{phox}-/-+OVA, DKOA= gp91^{phox}-MMP12 double knockout+alum, DKOO= gp91^{phox}-MMP12 double knockout+OVA. The results shown are pooled from 3 independent experiments. Counts were taken and averaged over 10 high power fields. Slides were counted on a Spencer AO light microscope at 40X magnification. Results are expressed as percent ± SEM. n= 5 animals/group. *denotes a p value<0.01 compared to post-OVA wildtype values.

3.7 Th2 cytokine release in airway

Cytokine concentrations present in the BALf were measured by ELISA. Fig. **7** shows 2.75-fold increase in IL-13 level in gp91^{phox}-/- mice post-OVA compared to WT post-OVA. IL-4 was increased All other Th2 cytokines showed values similar to post-OVA WT BALf. Table 4A shows that actual mRNA upregulation was 1.4-fold for IL-4 gene and 1.9-fold for IL-13 genes which are Th2 specific. There was also upregulation in IL-1α, IL-10 and IL-12α, the significance of which is not clear at this point. Cells secreting these are T cells, macs and some epithelial cells. Overall, IL-4: NOX-/- post OVA has 1.2-fold more protein and 2-fold more mRNA; IL-5: NOX-/- post OVA has 2-fold more protein and 2.8-fold more mRNA; IL-13: NOX-/- post OVA has 3-fold more protein and 5.6-fold more mRNA. Therefore, both by protein concentration and mRNA expression, Th2 cytokines show a manifold increase in gp91^{phox}-/- post-OVA compared to WT.

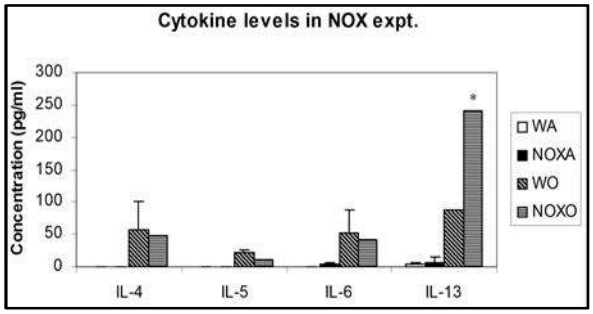

Fig. 7. Cytokine concentration in BALf. The concentration of cytokines in BALf was measured by outsourcing to Linco by multiplexing technique in a luminometer. Data expressed here are mean ± SEM. n=5/group. While all other Th2 cytokine levels were comparable to WT+OVA, IL-13 concentration was increased 2.7-fold over post-OVA WT values. Abbreviations used are: WT=wildtype, NOX=gp91^{phox}-/-, DKO=gp91^{phox}-MMP12 double knockout, WA=WT+alum, WO=WT+OVA, NOXA=gp91^{phox}-/-+alum, NOXO=gp91^{phox}-/-+OVA.

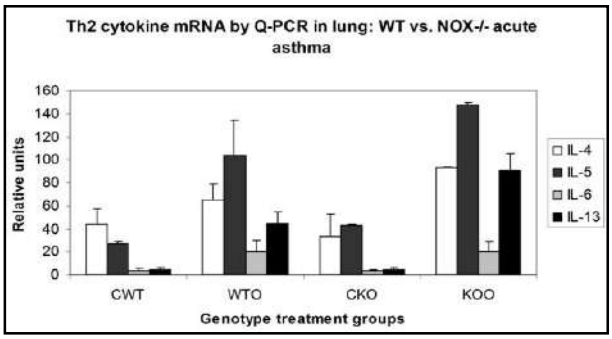

Data in Table 4a are presented in Graph.

Table 4A. Increase in gene expression of IL-1β, IL-10, IL-12 βand IL-13. Real-time PCR analysis shows expression of mRNA for the particular genes as calculated by relative index of Ct values normalized to GAPDH by real-time PCR. PCR was carried out using the comparative Ct method (Applied Biosystems software) with SYBR Green PCR core reagents (Applied Biosystems) and analysed using Applied Biosystems 7900HT Real-time PCR System software SDS 2.2.1. All primers used were specific to mouse. The graphs in* denote p value<0.01 compared to bleo-treated untransplanted group. Mean denotes the average of 2 independent experiments (n=4/group). Underlined numbers denote a mRNA expression in relative units normalized to mouse GAPDH that have p value<0.05 compared to wildtype post-OVA. Abbreviations used are: cWT= saline treated wildtype, WTO=wildtype post-OVA treatment, CKO=saline treated gp91^{phox} knockout, KOO= CKO=OVA treated gp91^{phox} knockout.

	Mean									
	IFN-γ	IL-1α	IL-1 β	IL-2	IL-4	IL-5	IL-6	IL-10	IL-12β	IL-13
CWT	4.67	71.27	3.79	2.57	44.26	27.15	3.59	4.21	7.27	4.72
WTO	4.96	411.67	21.17	65.56	65.42	103.45	20.04	23.61	21421.95	45.15
CKO	1.18	62.81	6.20	2.65	33.72	43.12	3.74	1.76	29.23	4.68
KOO	2.06	6037.51	33.65	8.63	92.78	147.74	20.58	134.96	306948.33	90.59
	SEM									
	IFN-γ	IL-1 α	IL-1 β	IL-2	IL-4	IL-5	IL-6	IL-10	IL-12β	IL-13
CWT	1.70	6.47	0.32	0.02	12.70	1.70	1.65	2.60	5.25	1.38
WTO	1.85	2.46	8.11	13.28	13.58	30.68	9.80	3.66	15756.71	9.45
CKO	0.27	0.68	1.58	1.61	19.35	0.90	0.96	0.65	21.91	1.32
KOO	0.60	5.50	1.74	1.72	1.02	1.42	8.28	3.43	107868.44	14.51

Table 4B. Increase in MCP-3 and VEGFb and decrease in TGFβ, VEGFa and VEGFc in post-OVA gp91^{phox}-/- lung. Real-time PCR data shows expression of mRNA for the particular genes as calculated by relative index of Ct values normalized to GAPDH by real-time PCR. PCR was carried out using the comparative Ct method (Applied Biosystems software) with SYBR Green PCR core reagents (Applied Biosystems) and analysed using Applied Biosystems 7900HT Real-time PCR System software SDS 2.2.1. All primers used were specific to mouse. The underlined number p value<0.01 compared to OVA-treated wildtype group. Abbreviations used are: cWT= saline treated wildtype, WTO=wildtype post-OVA treatment, CKO=saline treated gp91phox knockout, KOO= CKO=OVA treated gp91^{phox} knockout.

	Mean				
	MCP-3	TGFβ2	VEGFa	VEGFb	VEGFc
CWT	4.63	18.03	1973.06	176.39	2283.58
WTO	7.14	44.67	4260.86	334.59	4500.67
CKO	20901.40	32.88	34.40	106.73	15.11
KOO	166575.87	28.30	297.97	744.17	35.15
	SEM				
	MCP-3	TGFβ2	VEGFa	VEGFb	VEGFc
CWT	1.63	15.34	1549.62	2.24	1671.63
WTO	1.94	22.84	1982.14	3.56	1827.83
CKO	6361.97	9.71	13.79	80.67	0.97
KOO	119300.10	23.65	234.29	61.60	11.41

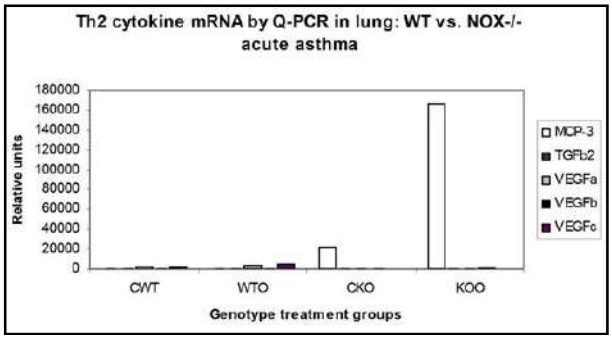

Data in Table 4B are presented in Graph.

3.8 Chemokine and growth factor gene expression

MCP-3 is a known macrophage chemotactic protein. Its gene expression was found to be upregulated manifolds both in the saline-treated control lung as well as post-OVA. The reason for this may be that in the absence of gp91phox, there is spontaneous upregulation of the chemokine gene. VEGFb was upregulated by 2.2-fold. Surprisingly, there was downregulation of TGFβ which might indicate that in keeping with decreased iNOS expression and the consequent shift in macrophage phenotype to M1 (killer) from M2 (healer), TGFβ expression was also downregulated corroborating once again that gp91phox may have a regulatory role in the development of Th2 phenotype and deletion of that disrupts the control or moderating effect involving cross-talk between T cells and the downstream phagocytes which need NADPH enzyme for the respiratory burst response and proliferation. Increased chemotaxis to MCP-1 may be explained by the increased expression of MCP-3. Upregulation of MMP12 in gp91^{phox}-/- both before and after OVA may indicate a compensatory mechanism in the regulation of Th2 response.

3.9 Expression of Rho kinase and MMPs associated with inflammation

Since this is an inflammatory response to the allergen, we hypothesized that other pro-inflammatory kinases and proteases may also be intimately involved in the pathway. Fig. 8 shows RT-PCR analysis of gene expression of Rho kinase, traditionally known to have anti-inflammatory functions, to be downregulated and so are MMP7, 10 and 28. The metalloproteases are also known regulators of inflammation and their down-regulation again corroborates that deletion of gp91phox may have disrupted a control mechanism on the development of Th2 mediated inflammation in the lung.

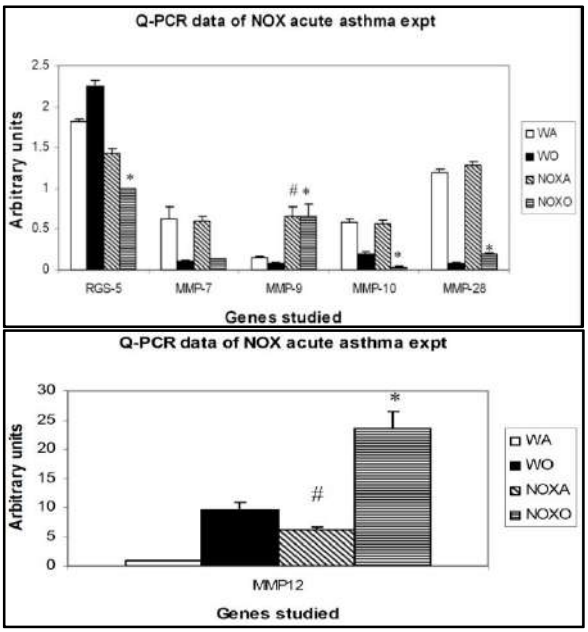

Fig. 8. Downregulation Rho kinase RGS-5 and MMP10 but upregulation of MMP9 and MMp28 mRNA post-OVA in KO mice compared to WT. Real-time PCR analysis was used to quantitate expression of mRNA for the particular genes as calculated by relative index of Ct values normalized to GAPDH by real-time PCR. PCR was carried out using the comparative Ct method (Applied Biosystems software) with SYBR Green PCR core reagents (Applied Biosystems) and analysed using Applied Biosystems 7900HT Real-time PCR System software SDS 2.2.1. All primers used were specific to mouse. *denotes p value<0.01 compared to WT+OVA values. # denotes p value<0.01 compared to WT+alum (control baseline values). n=5/group pooled from 2 experiments. Expression of the gene of interest was expressed in relative values normalized to the values obtained for mouse GAPDH. Compared to post-OVA WT values, Rho kinase RGS-5 mRNA was decreased 2.3-folds and MMp-10 3-fold, while MMP-9 was increased 8-fold and MMP-28 increased 2.3-fold (*denotes p value<0.05 compared to post-OVA WT).

3.10 Functionality of B cells

B cell function was tested by measuring OVA-specific IgE and IgG1 in post-OVA WT and the two KO mice. Fig. 9 shows that the values are comparable.

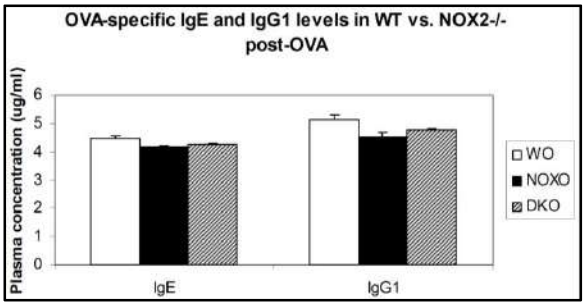

Fig. 9. Plasma concentrations of OVA-specific IgE and IgG1 are comparable between Wt and KO mice post-OVA. OVA-specific IgE and IgG1 were measured by standard ELISA using a capture and a detection antibody for each of the immunoglobulins. Data showed represents the mean of values pooled from three independent experiments (n=5/group). Abbreviations used are: WT=wildtype, NOX=gp91^{phox}-/-, DKO=gp91^{phox}-MMP12 double knockout, WO=WT+OVA, NOXO=gp91^{phox}-/-+OVA, DKOO= gp91^{phox}-MMP12 double knockout+OVA. Levels of OVA-specific cytokines in the alum-treated corresponding control groups were undetectable.

3.11 Functionality of T cells

Proliferation of MACS-purified (>86-92%) CD4+ and CD8+ splenocytes by MTT incorporation assay and OD measurement at 545nm of anti CD3/CD28 (0.01-1ug/ml) induced proliferation of CD4+ shows an 8.4-fold increase in post-OVA WT compared to a 7.4-fold increase in both KO mice. In CD8+ while post-OVA WT increased by 6.4-fold, the KO mice showed 7.9-fold increase compared to the corresponding saline-treated mice. With PMA/ionomycin (10ng/ml), CD4+ (post-OVA WT was 2.3-fold more than that in NOX-/-) while CD8+ was 1.5-fold more in post-OVA WT than in either KO mice. Overall, whereas proliferation of both T cell subsets to anti CD3/CD28 is comparable, response to PMA/ionomycin is somewhat compromised in KO post-OVA (Fig. 10A, B).

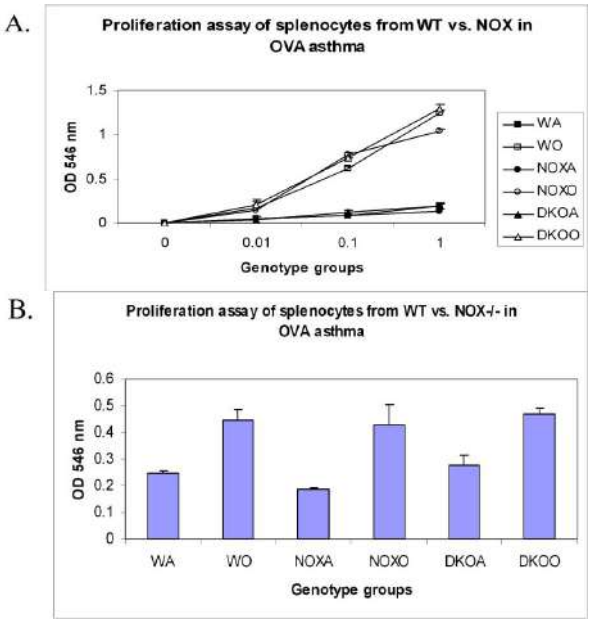

Fig. 10. T cells respond similarly to stimuli in Wildtype (WT) and knockout (KO) mice. A. Splenocytes from control (saline-treated) and OVA-treated mice were made into single cell suspensions in DMEM+10% heat-inactivated FCS. 0.1 Million cells were plated per well without and with increasing concentrations of anti-CD3 antibody and a constant concentration of anti-CD28 antibody (1μg/ml) and cultured for 3 days. **B.** 1μM PMA and 10ng/ml ionomycin were used to stimulate splenocytes from the above experimental mice and proliferation measured after 3 days. To measure proliferation, MTT assay called CellTiter96 (Promega) was used. OD 546 nm is directly proportional to the number of cells in culture. Abbreviations used are: WT=wildtype, NOX=gp91^{phox}-/-, DKO=gp91^{phox}-MMP12 double knockout, WA=WT+alum, WO=WT+OVA, NOXA=gp91^{phox}-/-+alum, NOXO=gp91^{phox}-/-+OVA, DKOA= gp91^{phox}-MMP12 double knockout+alum, DKOO= gp91^{phox}-MMP12 double knockout+OVA. The data presented are average of 3 independent experiments ± SEM. (n=5/group).

3.12 Functionality of macrophages

Macrophages and neutrophils are the ultimate downstream cells contributing to the asthma phenotype. Their functions are measured by the oxidative burst response to PMA and chemotaxis to MCP-1. Fig. 11 shows drastic downregulation of DHR+ cells by FACS gated on both Gr-1+ or F4/80+ populations showing either myeloid population to be incapable of showing respiratory burst response by generating reactive oxygen species by responding to PMA. Fig. 12 however, surprisingly shows upregulation in both gp91^{phox}-/- and DKO alveolar macrophages post-OVA. So here is a clear forking of signaling pathways regulating proliferation on the one hand, which was decreased in the KO mice (to PMA/Ionomycin), oxidative burst response which was drastically compromised (again to PMA) showing perhaps that the Protein kinase C pathway may be dysfunct in the absence of gp91^{phox} subunit of NADPH oxidase but when it comes to chemotaxis, there may be an upregulation of MCP-1 expaling the increase in actively migrating cells.

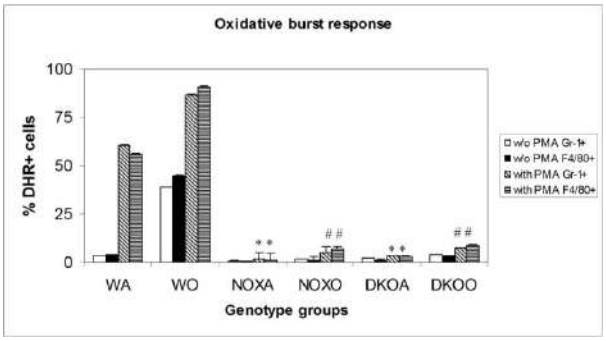

Fig. 11. Myeloid cells in BALf of both KO mice fail to respond to PMA. Alveolar leukocytes (0.5 x 10^6 cells) were stained with F4/80-Cy-Chrome and Gr1-APC for 30 min on ice, washed in PBS, warmed up at 37^{0}C for 5 min and loaded with 5mM dihydrorhodamine 123 (Molecular Probes, Eugene, OR). After 10 min at 370C, cells were split into two equal aliquots, and PMA (Sigma, St. Louis, MO) was added to one aliquot at a final concentration of 1mM. After 10 min incubation cells were washed in ice-cold PBS and immediately subjected to FACS analysis. Cells were gated on neutrophils (Gr1hi), or monocyte/macrophages (F4/80+) and percentage of cells positive for dihydrorhodamine 123 fluorescence with or without PMA treatment was determined for each gate. Results shown are mean of

3 independent experiments ± SEM. (n=5/group). * denotes p value<0.05 compared to WT without PMA treatment and # denotes p value<0.05 compared to WT post-PMA treatment. While WT cells respond to PMA before as well as after OVA challenge, cells from both KO mice before as well as after OVA, failed to respond appreciably. DHR was measured at Fluorescent channel 1 in using a BD FACScalibur and DHR+ cells (CD45+gated and Gr-1+ gated or F4/80+ gated) were analyzed using CellQuest Pro software.

3.13 T cell-macrophage crosstalk

Based on the aforementioned responses of T cells and macrophages it seems apparent that both cells are able to function well in response to OVA on their own at least as far as the asthma phenotype is concerned. They migrate in increased numbers from the blood and resident as well as recruited cells are found in impressive inflammatory exudates around the airways. So the next question was whether there is efficient cross-talk between the T cells upstream and the macrophages downstream. To this end, we did a mixed lymphocyte reaction using first the CD4+ T cells as the responders and the γ-irradiated alveolar macrophages as the stimulators from the experimental mice themselves and then used CD4+ T cells from splenocytes of BALB/c mice. Increase in proliferation measured by MTT assay (OD 570nm) shows increased T cell: APC interaction both when autologous APCs (macrophages from the adherent cell population in BALf of the same animal) were used and then APCs from experimental animals were used as stimulators to CD4+ T cells from the spleen of BALB/c mice which were the responders.

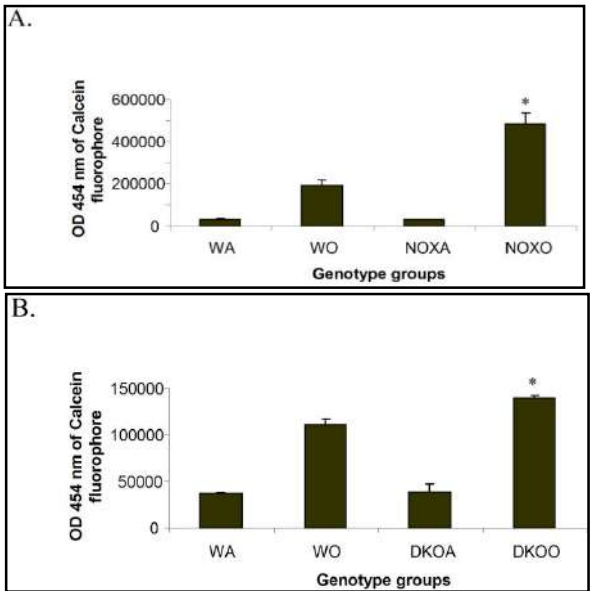

Fig. 12. MCP-1-driven chemotaxis of alveolar macrophages was increased in both KO mice post-OVA. 15mM MCP-1 was put in 29μl volume in the lower well and 10x106 alveolar macrophages (from 4 mice/experimental group), also in 29μl volume in the upper wells of a 96 well Neuroprobe CTX plates (Chemicon) in high glucose medium for 2 h followed by detachment by mechanical scraping and resuspension in Phenol red-free high glucose DMEM (Gibco) with 5% FBS with 0.5μg/ml Calcein-AM (1:2000 dilution) and incubation for 20 min at 37^{0}C. Migrated cells were quantified by fluorescence (excitation at 488 nm, emission at 520 nm) using a Victor 3V (Perkin Elmer laboratories) using a Wallac 1420 software. 2.5-fold and 1.26-fold increase in OD (proportionate to number of fluorescing cells in the upper well equivalent to the number of cells migrated) was found in post-OVA gp91^{phox}-/- and DKO mice respectively. * denotes p value<0.05 compared to values in OVA-treated wildtype group.

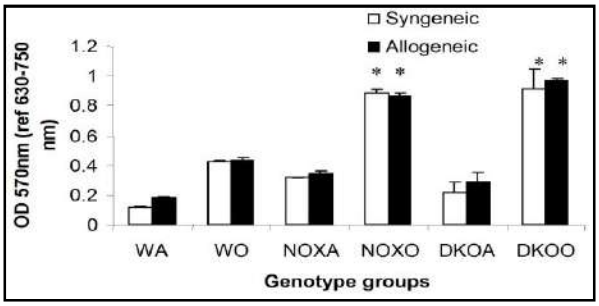

Fig. 13. Mixed lymphocyte reaction with CD4+ T cells and antigen presenting cells (APC) before and after OVA treatment. 0.1x105 CD4+ T cells isolated by magnetic activated cell separation (MACS) by positive selection from spleen of the mice were co-cultured with γ-irradiated 0.1x103 adhering alveolar macrophages from BALf of the same experimental animal. Both cell types were from the experimental animals themselves viz. C57Bl/6 WT and KO mice. This is Syngeneic MLR where the APCs (alveolar macrophages) were γ-irradiated (3300rads). Allogeneic MLR reaction involves co-culturing 0.1x105 CD4+ T cells from the spleen of BALB/c mice with 0.1x103 γ-irradiated APCs from BALf of the experimental mice. Both control (saline-treated) and OVA-treated of each group were tested. Each culture was incubated with 1μg/ml OVA. The responders here are the T cells and the stimulators are the APCs, viz. alveolar macrophages which are γ-irradiated to inhibit their own proliferation. Since acute allergic asthma is a Th2 mediated phenomenon, interaction between T cells and macrophages will elucidate functional cross-talk between the two cell types when responders are autologous as well as when they are from a different species. 2-fold increase in post-OVA NOX vs. post-OVA WT and 2.16-fold increase in post OVA-DKO vs. post-OVA shows that T cell: APC interaction is actually more efficient in the absence of the gp91^{phox} and MMP12 as well as gp91^{phox}.

3.14 iNOS expression

iNOS is a surface enzyme expressed by macrophages that are of the M1 or killer phenotype. Fig. 14 shows decrease in percent iNOS+ cells in PB, spleen, lung and BALf but not BM. This may indicate that there is a skewing of macrophage phenotype from killer to healer phenotype. This corroborates well with data in Fig. 11, 12 that these macrophages although migrating to the inflammatory focus in increased numbers are incapable of typical phagocytic functions which indicates a clear dichotomy in their signaling pathways.

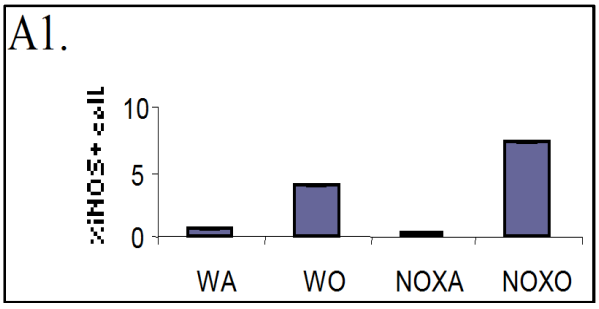

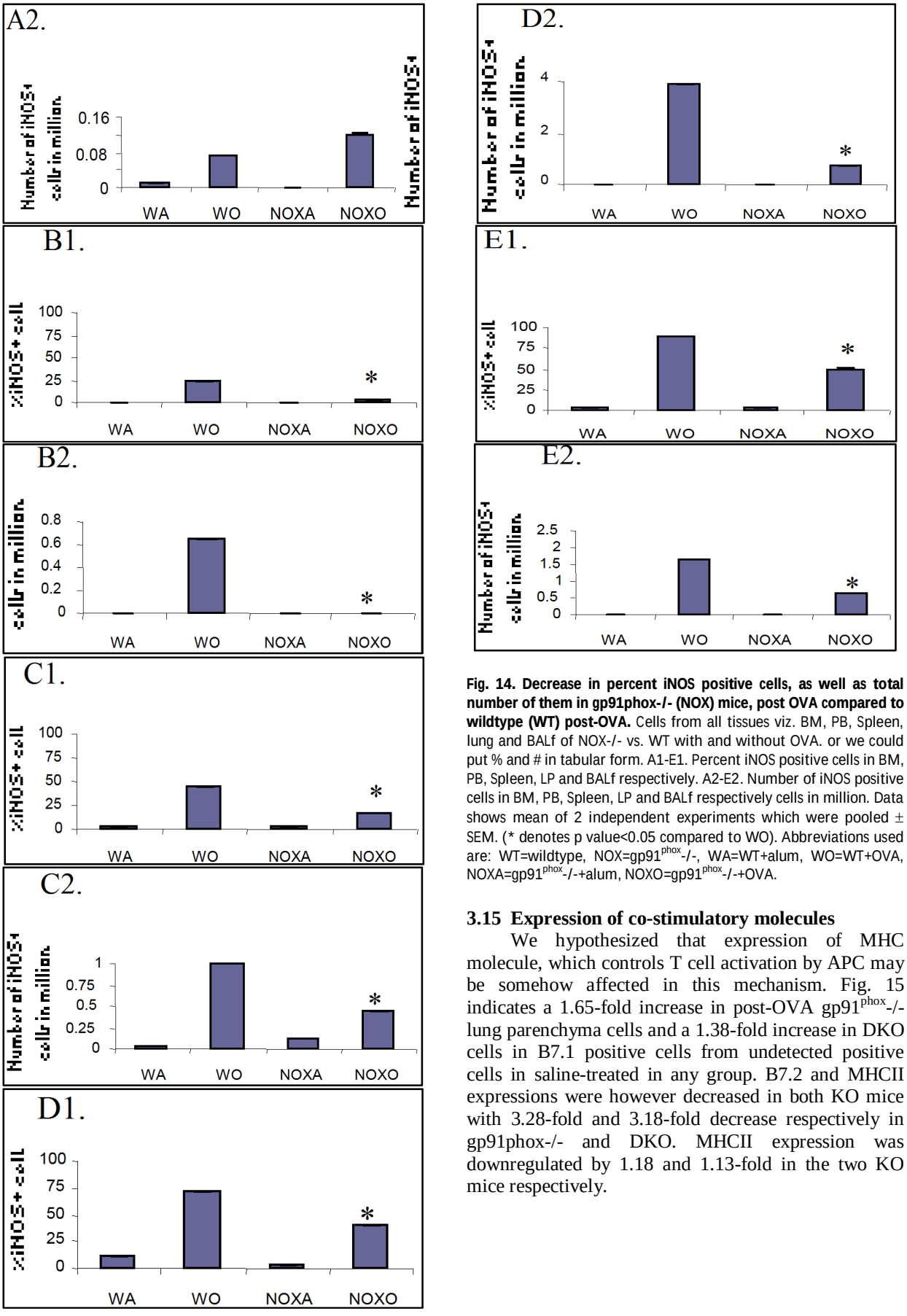

Fig. 14. Decrease in percent iNOS positive cells, as well as total number of them in gp91phox-/- (NOX) mice, post OVA compared to wildtype (WT) post-OVA. Cells from all tissues viz. BM, PB, Spleen, lung and BALf of NOX-/- vs. WT with and without OVA. or we could put % and # in tabular form. A1-E1. Percent iNOS positive cells in BM, PB, Spleen, LP and BALf respectively. A2-E2. Number of iNOS positive cells in BM, PB, Spleen, LP and BALf respectively cells in million. Data shows mean of 2 independent experiments which were pooled ± SEM. (* denotes p value<0.05 compared to WO). Abbreviations used are: WT=wildtype, NOX=gp91^{phox}-/-, WA=WT+alum, WO=WT+OVA, NOXA=gp91^{phox}-/-+alum, NOXO=gp91^{phox}-/-+OVA.

3.15 Expression of co-stimulatory molecules

We hypothesized that expression of MHC molecule, which controls T cell activation by APC may be somehow affected in this mechanism. Fig. 15 indicates a 1.65-fold increase in post-OVA gp91^{phox}-/- lung parenchyma cells and a 1.38-fold increase in DKO cells in B7.1 positive cells from undetected positive cells in saline-treated in any group. B7.2 and MHCII expressions were however decreased in both KO mice with 3.28-fold and 3.18-fold decrease respectively in gp91phox-/- and DKO. MHCII expression was downregulated by 1.18 and 1.13-fold in the two KO mice respectively.

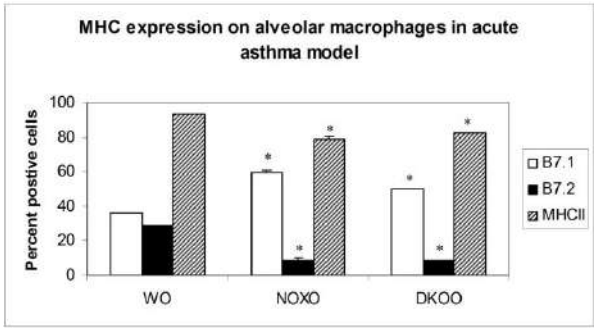

Fig. 15. Increase in B7.1 but decrease in B7.2 and MHCII expression in BAL cells. B7.1, B7.2 are co-stimulatory molecules expressed on alveolar macrophages and other antigen presentation cells like the dendritic cells and also B cells and monocytes. Expression of the said molecules was measured by FACS using specific fluorochrome-conjugated antibodies from Pharmingen. The data presented shows percent cells positive for the given antigen, expressed as mean ± SEM. n=4/group.

3.16 Bleomycin-induced fibrosis

Fig. 16 shows increase in soluble collagen content of whole lung in gp91^{phox}-/- but not DKO where values were similar to baseline showing that response did not occur. Gp91^{phox}-/- lung showed 1.3-folds increase in freshly synthesized collagen post-OVA compared to post-OVA WT. Histopathological staining with trichrome stain showed appreciable collagen deposits in WT and gp91phox post OVA but less in DKO lung (Panel A). A similar trend was found in picrosirius red stain (Panel C). Interestingly TGFβ staining was pronounced around the airways in WT and gp91^{phox}-/- post-OVA but not DKO.

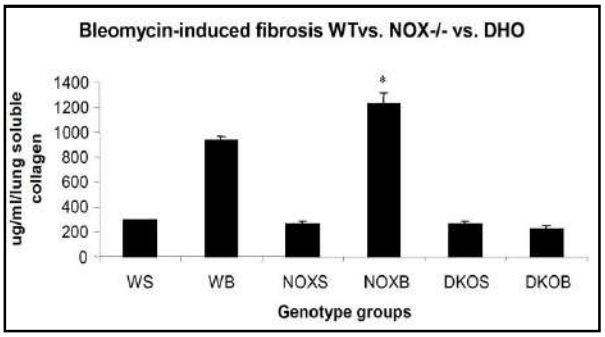

Fig. 16. Increase in collagen content of lung post-bleomycin in gp91^{phox}-/- but not in MM12-gp91^{phox} double knockout mice. Total collagen content freshly synthesized in the lung was measured by Sircol assay. Data represent mean of 2 independent experiments, n=4/group. Data are expressed as average ± SEM. * indicates the p value<0.05 compared to post-OVA value in wildtype mice. Abbreviations are: WS= saline-treated wildtype (baseline), WB=bleomycin-treated (single intra-tracheal dose of 0.075U/ml bleomycin and animals was sacrificed 14 and 21 d later. Here d21 data are shown), NOXS=saline-treated gp91phox null, NOXB=bleomycin-treated gp91phox null, DKOS=saline treated MMP12- gp91^{phox} double knockout, DKOB=bleomycin-treated MMP12- gp91^{phox} double knockout.

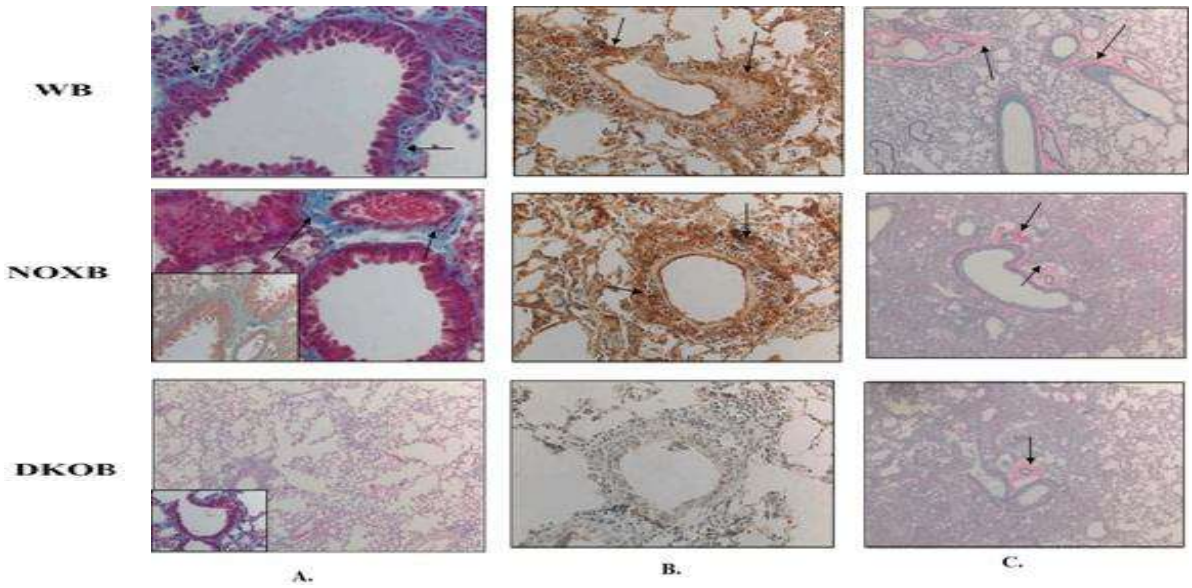

Fig. 17. Increased inflammation and fibrosis in lung of WT and gp91^{phox}-/- mice but not MMP12gp91^{phox} double knockout mice. 21d post-bleomycin treatment, mice were sacrificed and lungs were fixed overnight in 4% paraformaldehyde and embedded in paraffin. 8μ sections were stained by dyes (A, C. Masson's trichrome stain and picrosirius red respectively) and immunostained with TGFβ antibody and color developed by DAB (B). Arrows point at blue collagen deposits in panel A, TGFβ positive stain in panel B and to red collagen staining in panel C. In panel A, pinkish purple stains are that of cytoplasm and blue are the nuclei of inflammatory cells. Light blue stains are of collagenous deposits. While WT and gp91^{phox}-/- (designated as NOX-/- show increased collagen deposits and inflammation around airways post-OVA (all sections are those of post-OVA lung), MMP-12-gp91^{phox} double knockout lung shows minimum collagen deposition as well as TGFβ expression. While Panel A and B were at 60X magnification, Panel C was at 10X. Panel A inset shows another area of collagen deposition in bleo-treated wildtype (WB), NOXB and DKOB are bleo-treated gp01 phox-/- and double knockout respectively. The photomicrographs were taken in an Olympus VX4L microscope and Nikon digital camera. All photomicrographs were at 60X magnification.

3.17 Cells in BALf and lung post bleomycin over time

Total number of cells and cell subsets were measured periodically over time in WT, and the KO mice (Table 5A-D). Total cells were increased in bleomycin-treated NOX-/- mice at d7 after bleo with macrophages and lymphocytes contributing the most of the increase. PMNs also increased in percentage but total number was comparable to that in post-bleo WT. DKO, on the other hand, did not show a very low increase in the total number of cells over their saline-treated control group with lymphocytes and PMNs contributing to the slight increase entirely. Compared to saline treated WT, number of cells increased 6.6-folds a week after bleomycin treatment. This denuded at d14 and further at d21. So similar to previous data, cell number in BALf is actually not an indicator of the extent of fibrosis by d21. Similar trends were found in the lung (Table 5C). D7 probably signals the onset of fibrosis by increased cellular recruitment. Macrophages and T cells are the chief secretors of TGFβ traditionally thought to activate the collagen synthesis and deposition by alveolar epithelial cells. d8-21, therefore, is the scar tissue formation period when AEI has become denuded and so have AEII. This is shown in Table D where there is a progressive decrease in AEI through d21 while AEII first increased slightly only to equilibriate at d21. NOX-/- BALf showed a 1.7-fold increase in cell number which decreases predictably by d21. DKO BALf, however, shows no appreciable increase over saline treated either at d7 or at d21. Macrophages seem to be the chief cell populations accounting for this increase. In lung (Table 5C) however, on d7, a similar trend to that in BALf is found. The only difference is that both macrophages and lymphocytes make up for the increase.

Table 5A-D. Trends in cellular migration to BALf and Lung post-bleomycin over time and number of constitutive cells in lung. A-C represent CD45+ hematopoietic cells and D represent data on CD45- cells staining positive for alveolar epithelial cells. A. Number of cells in BALf a week after bleomycin treatment, B. Number of cells in BALf before and after bleo challenge where WT mice were assessed at d7, 14, and 21 and KO mice were assessed on d7 and d21, C. Number of cells in lung parenchyma (Lp) on d7 in all as no appreciable difference in cell numbers were found over time from d7-21, D. Number of cells in BALf of saline-treated and post-bleomycin (d7) wildtype (WT), gp91^{phox}-/- (NOX) and MMP12-gp91^{phox} double knockout (DKO) mice were assessed by Z1 Coulter particle counter from Beckman Coulter and differential counts done by specific fluorochrome antibody conjugates by FACS and by morphology in the light microscope. The data presented are mean ± SEM of 2 independent experiments (n=5/group).

CD45+ cells were gated and macrophages (Gr1-F4/80hi), lymphocytes (CD3+ and B220+), and neutrophils (Gr-1hi F4/80-) were identified, their percentages analyzed by CellQuest Pro and their total numbers calculated from the total number of cells obtained by lavage as described in materials and methods. The data presented is pooled from 2 independent experiments ± SEM. * denotes a p value<0.05 compared to WT post-bleo on corresponding time points. Abbreviations used are: WS=Wildtype (WT) +saline (d7), WB7= WT+post-bleomycin d7, WB14= WT+post-bleomycin d14, WB21= WT+post-bleomycin d21, NOXS=gp91^{phox}-/-+saline d21, NOXB21= gp91^{phox}-/-+bleomycin d21, DKOS= gp91^{phox}-MMP12 double knockout + saline (d21), DKOB21= gp91^{phox}-MMP12 double knockout + bleomycin (d21).

Table 5A. Number of cells in BALf after a week of Bleomycin treatment.

	WT saline (d7)	WT bleo (d7)	NOX saline (d7)	NOX bleo (d7)	DKO saline (d7)	DKO bleo (d7)
Total cell content (x10^5/ml)	4.27 ± 0.184	28.3 ± 0.224	4.515 ± 0.223	48.91* ± 1.59	2.61 ± 0.16	8.42 ± 0.13
Macrophages (x10^5/ml)	4.16 ± 0.57(97.2%)	11.14 ± 4.08(37.6%)	4.01 ± 0.31(89.9 %)	28.14* ± 6.83(57.4 7%)	1.87 ± 0.64(71.6 4%)	4.19 ± 3.18(49.8 2%)
Lymphocytes (x10^5/ml)	0.08 ± 0.01(2.0%)	12.63 ± 2.49(46.0%)	0.09 ± 0.02(2.01 %)	16.91* ± 3.65(34.5 3%)	12 ± 0.01(4.59 %)	1.44 ± 0.66(17.1 2%)
Neutrophils (x10^5/ml)	0.03 ± 0.01(0.7%)	4.5 ± 0.97(16.3%)	0.11 ± 0.01(0.02 %)	3.91 ± 0.53(7.98 %)	0.63 ± 0.14(24.1 3%)	2.78 ± 1.06(33%)

Table 5B. Number of CD45+ cells in BALf before and after bleomycin treatment (1 i.t. dose of 0.074 U/ml in 40µl volumes).

BALf	Mean							
10E5/ml	WS	WB7	WB14	WB21	NOXS	NOXB21	DKOS	DKOB21
Total cells	4.27	28.3	10.32	9.32	4.51	8.36	4.55	5.03
Macs	4.16	11.14	8.91	7.06	3.86	6.91	3.91	4.03
Lympho	0.08	12.63	1.76	1.33	1.32	2.43	1.44	0.56
PMN	0.03	4.5	0.41	0.87	0.67	1.02	0.67	0.41
	SEM							
10E5/ml	WS	WB7	WB14	WB21	NOXS	NOXB21	DKOS	DKOB21
Total cells	0.18	0.22	2.74	1.74	0.23	1.32	0.16	1.94
Macs	0.57	4.08	4.93	3.92	1.07	1.96	0.74	0.43
Lympho	0.01	2.49	0.67	0.67	0.54	0.43	0.32	0.21
PMN	0.01	0.97	0.07	0.32	0.32	0.22	0.11	0.13

Table 5C. Number of (CD45+) cells in LP before and after bleo treatment.

LP (d7)	Mean						SEM					
10E5/ml	WS	WB	NOXS	NOXB	DKOS	DKOB	WS	WB	NOXS	NOXB	DKOS	DKOB
Total cells	7.27	38.3	8.86	54.19*	6.85	9.56	0.07	4.04	0.08	2.6	0.27	0.65
Macs	6.16	22.14	7.13	31.38*	5.41	6.36	0.57	4.08	2.43	11.32	1.43	2.71
Lympho	1.08	9.63	0.97	21.41*	0.93	2.47	0.01	2.49	0.12	4.93	0.21	0.67
PMN	0.03	7.5	0.72	1.34	0.51	0.73	0.01	0.97	0.04	0.15	0.03	0.33
	Mean						SEM					
	CD45+											
%	WS	WB	NOXS	NOXB	DKOS	DKOB	WS	WB	NOXS	NOXB	DKOS	DKOB
Macs	84.73177	57.8068	80.474	57.90736	78.9781	66.5272	1.863	11.75	12.96	2.98	3.765	5.98
Lympho	14.85557	25.1436	10.9481	39.50913	13.57664	25.83682	2.84	4.96	1.95	3.67	3.98	8.43
PMN	0.412655	19.5822	8.12641	2.472781	7.445255	7.635983	0.043	6.73	2.07	1.09	1.97	2.06

Table 5D. Number of CD45+ cells counterstained with alveolar epithelial cells before and after bleomycin treatment.

	Mean CD45-				SEM			
	saline	bleomycin			saline	bleomycin		
WT	d21	d7	d14	d21	d21	d7	d14	d21
AEI	95.7	79.47	67.43	58.41	4.87	2.86	1.76	4.83
AEII	4.3	9.41	8.66	5.96	1.76	1.86	1.07	1.12
NOX-/-								
AEI	95.7	ND	ND	58.41	3.87	ND	ND	3.97
AEII	4.3	ND	ND	5.96	1.12	ND	ND	0.56
DKO								
AEI	95.7	ND	ND	97.41	4.16	ND	ND	3.87
AEII	4.3	ND	ND	4.96	0.56	ND	ND	1.87

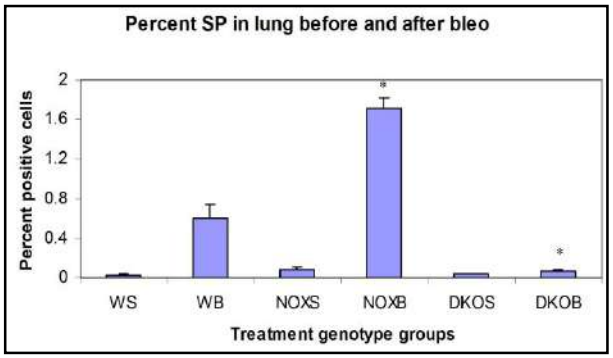

Fig. 18. Side population cells in lung before and after bleo in WT vs. KO mice. Side population cells were flow sorted by Hoechst dye effluxing cells from single cell suspension prepared by Dispase 1.2U/ml digested lung parenchyma incubated with 1:200 from Hoechst stock (aliquoted and frozen at - 20^{0}C in 370C water bath for 90 min and then flow sorted on FACSaria gating on a small (0.1%) cell population forming the characteristic "shoulder" OF actively dye-effluxing cells. The figure presents percent SP data in all three genotype groups before and after bleo treatment. The data presented is pooled from 2 independent experiments ±SEM. * denotes a p value<0.05 compared to WT post-bleo on d7. Abbreviations used are WS=Wildtype (WT) +saline (d7), WT=WT+post-bleomycin d7, NOXS=gp91 ^{phox}-/-+saline d7, NOXB= gp91 ^{phox}-/-+bleomycin d7, DKOS= gp91 ^{phox}-MMP12 double knockout + saline (d7), DKOB = gp91 ^{phox}-MMP12 double knock out + bleomycin (d7).

4. Discussion

Briefly, deletion of gp91^{phox} results in enhancement of composite asthma phenotype in mouse. Double deletion of gp91phoix and MMp12, a critical enzyme for phagocyte associated inflammation results in no alteration of the phenotype generated in the single deletion of gp91^{phox}-/-. There is a clear dichotomy in the macrophage function but overall, T cell function and macrophage functions are well coordinated. While inflammation in terms of inflammatory cell migration is enhanced, macrophage function downstream may not be all that bad. If gp91^{phox} is imagined to have a regulatory role in the development of the asthma phenotype, MMP12 seems to have a similar if not synergistic effect. These molecules are however not necessary for migration but are critical for PMA induced proliferation and MCP-1 induced chemotaxis. The overall Th2 response was enhanced possibly due to a lack of control over T cell: APC cross-talk in the KO mice as shown by MLR. Increased B7.1 but decreased B7.2 and MHCII expression may provide possible mechanisms for this regulatory function of gp91^{phox} and MMP12. On the other hand, in a predominantly macrophage perpetrated disease model of bleomycin-induced pulmonary fibrosis, gp91^{phox}-/- mouse shows the same trend of runaway inflammation and the resultant fibrosis but not so when MMP12 is deleted additionally. This may mean that while deletion of gp91phox may abolish the control mechanism required for keeping effects of bleomycin under check, additional deletion of MMP12 fails to elicit any effect of bleomycin after 21 days of treatment when fibrosis is fully developed. Therefore MMP12 may be critical for phagocytes to process signals necessary for a) increased AEI and AEII mortality, b) increased collagen synthesis, and c) inflammation, the first step for accumulation the cell populations in lung and BALf to initiate the onset and development of the fibrotic process itself.

The results described above indicate that gp91^{phox}-/- mice respond to OVA in a more exaggerated fashion compared to WT post-OVA, in terms of total

number of cells migrated to the lung (1.8 folds) and BALf (1.7 folds), although the total number of cells in bone marrow (obtained from two femurs) and that in circulating peripheral blood were comparable. Expressed as a fraction of circulating cells recruited into the lungs and BALf in response to allergic immune response, both knockout mice seem to show similar trends. Cell subsets for which recruitment index is more than 1, indicate a cumulative effect where both cells from circulation as well as resident cells normally present in the pulmonary milieu in surveillance, seem to be equally important. Recruitment of B cells, monocytes, neutrophils and basophils are increased in the lungs of both knockout mice compared to post-OVA wildtype while that of T cells, neutrophils and basophils in BALf are increased in the knockout vs. the OVA-treated wildtype (Table 2B).

MMP-9 is known to play a role in the migration and inflammatory responses by Eos and PMN, and control repair responses in asthma, especially in the resolution of allergic inflammation. So upregulation of MMP-9 gene in upon $gp91^{phox}$ deletion and also post-OVA treatment of the knockout mouse, cannot be explained easily. It may either have a protective role which is confounded upon deletion of gp91phox or it may be a compensatory mechanism in reaction to the deletion of the same. Any complementary role of this metalloprotease with the subunit of NADPH oxidase is unknown. MMP-12, on the other hand, controls the migration of monocytes and macrophages to inflammatory sites and airway remodeling by degrading ECM proteins [18]. It is supposed to have a protective effect in emphysema [19].

B7.1, a co-stimulatory signal necessary for the activation of T cells, can be expressed on the cell surface by B cells, dendritic cells and macrophages, the antigen presenting cells. It is associated with activation of cell-mediated response, especially Th2 response. At baseline, they are not expressed but upon activation are upregulated. In our model, upregulation of B7.1 but downregulation of B7.2 and MHCII shows a possible mechanism by which gp91phox and MMP12, may synergistically regulate Th2 responsiveness and deletion of the same disrupts this pathway.

Mature T lymphocytes become activated to perform their effector functions when stimulated by appropriate APC bearing MHC class I or class II molecules. They require both antigen-specific and immunoregulatory signals for optimum activation. The first signal comes from the T cell receptor as it recognizes antigenic peptides presented by MHC molecules. A variety of co-stimulatory receptors provide the second signal when they interact with ligands on APCs. The B7 family of ligands and their receptors is important in pathways of co-stimulation and inhibition if immune responses. B7.1 and B7.2 are co-stimulatory molecules capable of turning on the immune system by regulating antigen-specific activation and proliferation of lymphocytes and play a critical role in regulating the immune system. Appropriate co-stimulation may alter the number and strength of MHC-peptide-TCr complexes necessary for T cell activation. It may also complement the intracellular signals sent via T cell receptors and help T cells adhere to APCs to promote MHC-peptide-TCR interaction. These MHC molecules bind TCR and simultaneously engage either CD8 or CD4. T cell activation and differentiation requires not only TCR recognition of the antigen-MHC complex, but also costimulation through the interaction of accessory molecules on APC and their corresponding receptors on T cells. CD28 is an important costimulatory receptor on T cells and binds to CD80 (B7-1) and CD86 (B7-2) on activated APC [20,21]. The crucial role played by CD28 in the proliferation and differentiation of T cells has been highlighted by studies using CD28 knockout mice. However, some immune responses remain intact in the absence of CD28, perhaps because a prolonged TCR signal overcomes the need for costimulation, and/or other costimulatory molecules can substitute for CD28 [22,23]. Additional T cell costimulatory molecules, *i.e*. ICOS, were identified, and have functions similar to, but not completely overlapping with, CD28. ICOS is not expressed by resting T cells, but is induced after T cell activation and is important for T cell activation and effector function [24,25]. ICOS costimulation failed to significantly up-regulate IL-2; however, it up-regulated the secretion of IL-4, IL-5, IFN-γ, TNF-α and GM-CSF to 50-70% of the levels achieved with CD28 costimulation [26]. Following cellular activation, lymphocytes can differentiate into Th1 or Th2 cells according to the type of cytokine they produce, the balance of which will ultimately determine the outcome of the cellular response. Typically, production of IFN-γ and IL-12 will favor a Th1 response, whereas presence of IL-4and IL-10 will determine a Th2 pattern. In HP no clear pattern of polarization has been defined. In experimental models, Th1 responses may be important since Th1 $CD4^+$ cells can adoptively transfer the disease to healthy animals [26]; IFN-γ and IL-12 may also play a role in the pathogenesis of HP in mice [27,28], but in human HP, recent studies suggest that a Th2-type response is predominant [29,30]. T cell activation requires at least two distinct signals [31]; the first is Ag-specific and is delivered through the engagement of TCRs. The second signal is mediated by the interaction of costimulatory molecules present on APCs with their ligands on T cells. The B7:CD28/CTLA4 is a major pathway which provides these potent signals, crucial for complete T cell activation. CD28 and CTLA4 are ligands for B7-1 and B7-2. These ligands bind to both B7 but with different avidities, CTLA4 binding is 20-to 100-fold higher than CD28. This difference in avidity has been exploited to block B7-CD28 interactions by the use of CTLA4-Ig, a soluble fusion protein made from the

extracellular portion of CTLA4 linked to the Fc portion of IgG [32]. Furthermore, B7/CD28 costimulatory pathway may influence not only the extent of T cell activation but also the regulation of T cell differentiation [33]. Depending on the system studied, B7 costimulation has been shown to influence both Th1 and Th2 cytokine production [34]. In the normal lung, alveolar macrophages (AM) have a low expression of B7 molecules and a poor capacity to function as APCs [35]. So antagonistic alterations in B7 family of receptors in the acute asthma pathway may indicate a definite role for either gp91phox or both gp91phox and MMP12 in controlling the co-stimulatory activating pathway in T cell activation in Th2 response. The role of MMP12 and $gp91^{phox}$ are however probably completely different in bleomycin-induced fibrosis and need further study.

Acknowledgments

This work was supported by the National Institute of Health grants 62-9208 and 62-9538 (WRH). We thank J.W. Heinecke for the Cybb-/- mice that were bred in his laboratory by Z. Sagawa, and G.K.S. Chiang for technical assistance with the whole body plethysmography, and R. Norris for editing the manuscript. Tim Burkland and Eman Sadoun respectively did the real-time PCR analysis of the MMP and RGS genes.

References

[1]. Groemping, Y., and Rittinger, K. (2005). Activation and assembly of the NADPH oxidase: a structural perspective. *Biochem. J.*, 386: 401–416.

[2]. Henriet, S.S., Hermans, P.W., Verweij, P.E., Simonetti, E., Holland, S.M., Sugui, J.A., Kwon-Chung, K.J., Warris, A. (2010). Human leukocytes kill *Aspergillus nidulans* by ROS-independent mechanisms. *Infect. Immun.*, 79(2):767-73.

[3]. Bylund, J., Brown, K.L., Movitz, C., Dahlgren, C., Karlsson, A. (2010). Intracellular generation of superoxide by the phagocyte NADPH oxidase: How, where, and what for? *Free Radic. Biol. Med.*, 49(12):1834-45.

[4]. Kumar, S., Patel, S., Jyoti, A., Keshari, R.S., Verma, A., Barthwal, M.K., Dikshit, M. (2010). Nitric oxide-mediated augmentation of neutrophil reactive oxygen and nitrogen species formation: Critical use of probes. *Cytometry A.*, 77(11):1038-48.

[5]. De Ravin, S.S., Zarember, K.A., Long-Priel, D., Chan, K.C., Fox, S.D., Gallin, J.I., Kuhns, D.B., Malech, H.L. (2010). Tryptophan/kynurenine metabolism in human leukocytes is independent of superoxide and is fully maintained in chronic granulomatous disease. *Blood*, 116(10):1755-60.

[6]. Chan, E.C., Dusting, G.J., Guo, N., Peshavariya, H.M., Taylor, C.J., Dilley, R., Narumiya, S., Jiang, F. (2010). Prostacyclin receptor suppresses cardiac fibrosis: role of CREB phosphorylation. *J. Mol. Cell. Cardiol.*, 49(2):176-85.

[7]. Leverence, J.T., Medhora, M., Konduri, G.G., Sampath, V. (2010). Lipopolysaccharide-induced cytokine expression in alveolar epithelial cells: Role of PKCζ-mediated p47phox phosphorylation. *Chem. Biol. Interact.*, 189(1-2):72-81.

[8]. Kim, Y., Zhou, M., Moy, S., Morales, J., Cunningham, M.A., Joachimiak, A. (2010). High-resolution structure of the nitrile reductase QueF combined with molecular simulations provide insight into enzyme mechanism. *J. Mol. Biol.*, 404(1):127-37.

[9]. Santilli, G., Almarza, E., Brendel, C., Choi, U., Beilin, C., Blundell, M.P., Haria, S., Parsley, K.L., Kinnon, C., Malech, H.L., Bueren, J.A., Grez, M., Thrasher, A.J. (2010). Biochemical Correction of X-CGD by a Novel Chimeric Promoter Regulating High Levels of Transgene Expression in Myeloid Cells. *Mol. Ther.*, 19(1):122-32.

[10]. Kassim, S.Y., Fu, X., Liles, W.C., Shapiro, S.D., Parks, W.C., Heinecke, J.W. (2005). NADPH oxidase restrains the matrix metalloproteinase activity of macrophages. *J. Biol. Chem.*, 280(34):30201-5.

[11]. Pollock, J.D., Williams, D.A., Gifford, M.A., Li, L.L., Du, X., Fisherman, J., Orkin, S.H., Doerschuk, C.M., Dinauer, M.C. (1995). Mouse model of X-linked chronic granulomatous disease, an inherited defect in phagocyte superoxide production. *Nat. Genet.*, 9, 202-9.

[12]. Shipley, J.M., Wesselschmidt, R.L., Kobayashi, D.K., Ley, T.J., Shapiro, S.D. (1996). Metalloelastase is required for macrophage-mediated proteolysis and matrix invasion in mice. *Proc. Natl. Acad. Sci. U. S. A.*, 93: 3942–3946.

[13]. Ena Ray Banerjee, Yi Jiang, William R. Henderson, Jr, Yvette Latchman, and Thalia Papayannopoulou (2009). Absence of α4 but not β2 integrins restrains the development of chronic allergic asthma using mouse genetic models. *Exp. Hematol.*, 37: 715–727.

[14]. Ena R. Banerjee, Yvette E. Latchman, Yi Jiang, Greg V. Priestley, and Thalia Papayannopoulou (2008). Distinct changes in adult lymphopoiesis in Rag2-/- mice fully reconstituted by α4-deficient adult bone marrow cells. *Exp. Hematol.*, 36(8):1004-13.

[15]. Ulyanova, T., Priestley, G.V., Banerjee, E.R., Papayannopoulou, T. (2007). Unique and redundant roles of alpha4 and beta2 integrins in

kinetics of recruitment of lymphoid vs myeloid cell subsets to the inflamed peritoneum revealed by studies of genetically deficient mice. *Exp. hematol*., 35(8): 1256-65.

[16]. Banerjee, E.R., Jiang, Y., Henderson, W.R. Jr, Scott, L.M., Papayannopoulou, T. (2007). Alpha4 and beta2 integrins have nonredundant roles in asthma development, but for optimal allergen sensitization only alpha4 is critical. *Exp. Hematol.*, 35(4): 605-17.

[17]. William, R., Henderson, Ena Ray Banerjee, and Emil Y. Chi (2005). Differential Effects of (S)- and (R)-enantiomers of albuterol in mouse asthma Model. *Journal of Allergy and Clinical Immunology*, 116: 332-40.

[18]. Sophie Lanone, Tao Zheng, Zhou Zhu, Wei Liu, Chun Geun Lee, Bing Ma, Qingsheng Chen, Robert J. Homer, Jingming Wang, Lesley A. Rabach, Morgan E. Rabach, J. Michael Shipley, Steven D. Shapiro, Robert M. Senior, and Jack A. Elias (2002). Overlapping and enzyme-specific contributions of matrix metalloproteinases-9 and -12 in IL-13–induced inflammation and remodeling. *J. Clin. Invest.*, 110(4):463–474.

[19]. Roza, I. Nurieva, Xoi Moui Mai, Katherine Forbush, Michael J. Bevan and Chen Dong (2003). B7h is required for T cell activation, differentiation, and effector function. *PNAS*, 100: 14163-14168.

[20]. Shengdian Wang., Gefeng Zhu., Andrei I., Chapoval., Haidong Dong., Koji Tamada., Jian Ni and LiepingChe (2000). Costimulation of T cells by B7-H2, a B7-like molecule that binds ICOS. *Blood*, Vol. 96, No. 8, pp. 2808-281.

[21]. Suh, W.K., Tafuri, A., Berg-Brown, N.N., Shahinian, A., Plyte, S., Duncan, G.S., Okada, H., Wakeham, A., Odermatt, B., Ohashi, P., Mak, T.W. (2004). The inducible costimulator plays the major costimulatory role in humoral immune responses in the absence of CD28. *J. Immunol.*, 172(10):5917- 23.

[22]. Hutloff, A., Dittrich, A.M., Beier, K.C., Eljaschewitsch, B., Kraft, R., Anagnostopoulos, I., Kroczek, R.A. (1999). ICOS is an inducible T-cell co-stimulator structurally and functionally related to CD28. *Nature*, 397(6716):263-6.

[23]. Yoshinaga, S.K. Whoriskey, J.S., Khare, S.D., Sarmiento, U., Guo, J., Horan, T., Shih, G. *et al.*, (1999). T-cell co-stimulation through B7RP-1 and ICOS. *Nature*, 402(6763):827-32.

[24]. Qian, X., Agematsu, K., Freeman, G.J., Tagawa, Y., Sugane, K., Hayashi, T. (2006). The ICOS-ligand B7-H2, expressed on human type II alveolar epithelial cells, plays a role in the pulmonary host defense system. *Eur. J. Immunol.*, 36(4):906-18.

[25]. M. Schuyler., K. Gott and B. Edwards (1999). Th1 Cells That Adoptively Transfer Experimental Hypersensitivity Pneumonitis Are Activated Memory Cells. *Lung*, 177(6): 377-89.

[26]. Gudmundsson, G., Hunninghake, G.W. (1997). Interferon-gamma is necessary for the expression of hypersensitivity pneumonitis. *J. Clin. Invest.*, 99:2386-2390.

[27]. Gunnar Gudmundsson, Martha M. Monick and Gary W. Hunninghake (1998). IL-12 Modulates Expression of Hypersensitivity Pneumonitis. *J. Immunol.*, 161(2):991-9.

[28]. Boyd G.C., McSharry, K., McLeod, S., Sriram, and F. Boyd (1999). Lymphocyte responses in pigeon breeders with extrinsic allergic alveolitis/hypersensitivity pneumonitis (EAA/HP) are predominantly T helper 2-type. *Am. J. Respir. Crit. Care Med.*, 159:A742.

[29]. Meyer, F., Ramanujam, K.S., Gobert, A.P., James, S.P. and Wilson, K.T. (2003). Cyclooxygenase-2 activation suppresses Th1 polarization in response to *Helicobacter pylori*. *J. Immunol.*, 171:3913-7.

[30]. Lenschow, D.J., T.L. Walunas., J.A. Bluestone. (1996). CD28/B7 system of T cell costimulation. *Annu. Rev. Immunol.*, 14:233-58.

[31]. Linsley, P.S., P.M. Wallace., J. Johnson., M.G. Gibson., J.L. Greene., J.A. Ledbetter., C. Singh., M.A. Tepper (1992). Immunosuppression *in vivo* by a soluble form of the CTLA-4 T cell activation molecule. *Science*, 257:792-5.

[32]. Thompson, C.B. (1995). Distinct roles for the costimulatory ligands B7-1 and B7-2 in T helper cell differentiation? *Cell*, 81(7):979-82.

[33]. Schweitzer, A.N., Sharpe, A.H. (1998). Studies using antigen-presenting cells lacking expression of both B7-1 (CD80) and B7-2 (CD86) show distinct requirements for B7 molecules during priming versus restimulation of Th2 but not Th1 cytokine production. *J. Immunol.*, 161:2762-2771.

[34]. Chelen, C.J., Fang, Y., Freeman, G.J., Secrist, H., Marshall, J.D., Hwang, P.T., Frankel, L.R., DeKruyff, R.H., Umetsu, D.T. (1995). Human alveolar macrophages present antigen ineffectively due to defective expression of B7 costimulatory cell surface molecules. *J. Clin. Invest.*, 95(3):1415-21.

Abbreviations: OVA, ovalbumin; BM, bone marrow; PB, peripheral blood; BALf, bronchoalveolar lavage fluid; LP, lung parenchyma; AHR, airway hyper-reactivity/responsiveness; i.t., intra-tracheal; i.v., intravenous; i.p., intraperitoneal; H&E, Hematoxylin and Eosin; Penh, enhanced pause; WBP, whole body plethysmography; KO, knockout; ROS, reactive oxygen species; NOX, NADPH oxidase.